Acta Pharmaceutica Sinica B 2025;15(8):4248−4264

Chinese Pharmaceutical Association
Institute of Materia Medica, Chinese Academy of Medical Sciences

Acta Pharmaceutica Sinica B

www.elsevier.com/locate/apsb
www.sciencedirect.com

ORIGINAL ARTICLE

Artificial mesenchymal stem cell extracellular vesicles enhanced ischemic stroke treatment through targeted remodeling brain microvascular endothelial cells

Shengnan Li[a,b,†], Wei Lv[c,†], Jiangna Xu[a,b], Jiaqing Yin[a,b], Yuqin Chen[a,b], Linfeng Liu[a,b], Xiang Cao[a], Wenjing Li[d], Zhen Li[d,*], Hua Chen[e,*], Hongliang Xin[a,b,*]

[a]*Department of Pharmaceutics, School of Pharmacy, Nanjing Medical University, Nanjing 211166, China*
[b]*Department of Radiology, the Affiliated Wuxi People's Hospital of Nanjing Medical University, Wuxi People's Hospital, Wuxi Medical Center of Nanjing Medical University, Wuxi 214023, China*
[c]*Department of Pharmacy, the Affiliated Jiangyin Hospital of Xuzhou Medical University, Wuxi 214400, China*
[d]*College of Pharmacy, Dalian Medical University, Dalian 116044, China*
[e]*Department of Neurosurgery, the First Affiliated Hospital with Nanjing Medical University, Nanjing 210029, China*

Received 17 January 2025; received in revised form 4 March 2025; accepted 29 April 2025

KEY WORDS

Artificial extracellular vesicles;
Mesenchymal stem cell membrane proteins;
miR-132-3p;
Cerebral vascular endothelial cells;
Blood−brain barrier;
Oxidative stress;

Abstract Ischemic stroke is the leading cause of disability and mortality worldwide. The blood−brain barrier (BBB) is the first line of defense after ischemic stroke. Disruption of the BBB induced by brain microvascular endothelial cells (BMECs) dysfunction is a key event that triggers secondary damage to the central nervous system, where blood-borne fluids and immune cells penetrate the brain parenchyma, causing cerebral edema and inflammatory response and further aggravating brain damage. Here, we develop a novel artificial mesenchymal stem cell (MSC) extracellular vesicles by integrating MSC membrane proteins into liposomal bilayers, which encapsulated miR-132-3p with protective effects on BMECs. The artificial extracellular vesicles (MSCo/miR-132-3p) had low immunogenicity to reduce non-specific clearance by the mononuclear phagocytosis system (MPS) and could target ischemia-

*Corresponding authors.
E-mail addresses: lizhenpharm@126.com (Zhen Li), chenhua@njmu.edu.cn (Hua Chen), xhl@njmu.edu.cn (Hongliang Xin).
[†]These authors made equal contributions to this work.

Peer review under the responsibility of Chinese Pharmaceutical Association and Institute of Materia Medica, Chinese Academy of Medical Sciences.

https://doi.org/10.1016/j.apsb.2025.06.009

Apoptosis;
Ischemic stroke therapy

injured BMECs. After internalization into the damaged BMECs, MSCo/miR-132-3p escaped the lysosomes *via* the H_{II} phase transition of 1,2-dioleoyl-*sn*-glycero-3-phosphoethanolamine (DOPE) and decreased cellular reactive oxygen species (ROS) and apoptosis levels by regulating the RASA1/RAS/PI3K/AKT signaling pathway. In the transient middle cerebral artery occlusion (tMCAO) models, MSCo/miR-132-3p targeted impaired brain regions (approximately 9 times the accumulation of plain liposomes at 12 h), reduced cerebral vascular disruption, protected BBB integrity, and decreased infarct volume (from 44.95% to 6.99%).

1. Introduction

Stroke is a serious cerebrovascular disease causing permanent disability and death worldwide, with ischemic stroke accounting for about 87%[1]. Tissue-type plasminogen activator (t-PA) is currently the only drug approved by the U.S. Food and Drug Administration (FDA) for the treatment of acute ischemic stroke. However, its use is limited by a narrow therapeutic window, bleeding risks, and contraindications[2,3]. Additionally, the therapeutic effect of cerebral ischemia-reperfusion injury determines the survival time and quality of life of stroke survivors. Unfortunately, no neuroprotectant has been approved by the FDA so far. Although most preclinical studies have shown positive therapeutic effects of neuroprotective drugs in animal models of ischemia stroke, very few phase III clinical trials have yielded satisfactory results because of the impediment of the blood−brain barrier (BBB) to drug delivery and serious off-target toxicity[4]. Therefore, there is an urgent need to explore safe and effective strategies for cerebral ischemic injury treatment.

Located at the interface between the peripheral circulation and the brain parenchyma, the BBB acts as a dynamic "gatekeeper", regulating molecular transport, preventing the invasion of circulating pathogens, and is critical for maintaining homeostasis in the brain microenvironment[5,6]. When ischemia stroke occurs, BBB dysfunction emerges immediately and lasts for several weeks, which leads to a series of severe secondary injuries such as cerebral edema, neuroinflammation, neuronal death induced by the inflow of fluids, toxins, and a wide range of immune cells and inflammatory factors from the blood into the brain parenchyma[7]. As the most important component of the BBB, brain microvascular endothelial cells (BMECs) are held together by tight junction proteins, forming a "switch" that constrains BBB permeability[6,8]. Once cerebral ischemia-reperfusion occurs, inflammation develops within the vessel, contributing to oxidative stress and apoptosis of BMECs and the breakdown of tight junctions, accompanied by BBB integrity destruction, which in turn exacerbates ischemic injury to brain tissue[9-11]. Therefore, BMECs are promising therapeutic targets that are essential for mitigating ischemic/reperfusion (IR) brain injury.

As an endothelial-specific microRNA (miRNA), miR-132-3p is a pivotal regulator of angiogenesis, playing a role in endothelial dysfunction, angiogenesis, and cerebrovascular disease through targeted p120RAS-GTPase activating protein (p120RASGAP, RASA1)[12-14], which inactivates RAS by enhancing its intrinsic GTPase activity and is a key negative modulator of vascular development and remodeling[15-17]. miR-132-3p has a great protective effect on neurovascularity during the acute phase of ischemia stroke by decreasing ROS generation and apoptosis in the injured BMECs, enhancing the expression of tight junction proteins, and restoring the barrier function of the BBB[18-20]. However, *in vivo* delivery of miRNAs still confronts multiple challenges: (1) miRNAs are readily degraded by nuclease enzymes that are widely distributed in body fluids[21]. (2) Exogenous miRNAs are immunogenic and prone to be scavenged by the mononuclear phagocytosis system (MPS) [22]. (3) There is electrostatic repulsion between the negatively charged miRNAs and the cell membrane, accounting for poor cellular uptake[23]. (4) The delivery of miRNAs is still plagued by off-target side effects and poor lysosomal escape capability[24]. Consequently, it is extremely crucial to develop a target drug delivery system for ischemia stroke treatment by miRNA.

Extracellular vesicles are a class of membranous structures secreted into the extracellular space comprising exosomes (30−150 nm) and microvesicles (50−1000 nm)[25], which originate from the endosomal system or are shed from the plasma membrane, respectively[26,27]. As intercellular communication messengers, nanoscale extracellular vesicles can selectively transport bioactive components (including proteins, lipids, and nucleic acids) of parental cells and protect them from degradation, affecting various physiological and pathological processes[28]. Depending on the plasma membrane of different cellular origins, extracellular vesicles express different surface markers that determine their interactions with receptor cells and confer their intrinsic targeting ability[29]. For example, mesenchymal stem cell (MSC)-derived extracellular vesicles express the MSC-specific markers CXCR4 and VCAM-1, which mediate their homing and adhesion to injured vascular endothelial cells[30,31]. In addition, extracellular vesicles can be engineered by various means, such as surface modification of targeting peptides, genetically engineering overexpression of a protein, and physical or chemical loading of a drug, which can increase their selective targeting ability and therapeutic effect[32]. Therefore, extracellular vesicles are extremely promising as targeted drug delivery system[33]. The use of red-cell-derived extracellular vesicles to deliver RNA drugs, including antisense oligonucleotide, Cas9 mRNA, and guide RNA, showed highly robust microRNA inhibition and CRISPR-Cas9 genome editing without obvious cytotoxicity in both human cells and xenograft mouse models[34]. However, natural extracellular vesicles as biological carriers still face great challenges, such as difficult enrichment, low yield, lack of standardized methods, and difficulty in large-scale production and quality control[35]. Accordingly, the development of artificial extracellular vesicles can accelerate the clinical translation of extracellular vesicles as a targeted drug delivery system.

Herein, we developed an artificial MSC extracellular vesicle by combining formulation technology to deliver miR-132-3p for

ischemic stroke treatment. The artificial MSC extracellular vesicles system (designated MSCo/miR-132-3p) was fabricated by integrating MSC-specific membrane proteins into liposomal phospholipid bilayers *via* membrane protein insertion method and loading the hydrophilic core with protamine-compressed miR-132-3p. This artificial MSC extracellular vesicle could retain the superiority of MSC extracellular vesicles as carriers while avoiding their drawbacks. It can inherit the biocompatibility, long-circulating property, and lesion targeting ability of parental MSCs, and also has the controllability of preparation, homogeneity, stability of physicochemical properties, and adjustability of cargo loading and release of nanocarriers. As illustrated in Fig. 1, MSCo/miR-132-3p artificial nanovesicles can circumvent the clearance of the body's immune system and prolong the circulation time with the action of CD47 protein on the surface, initiate migration through the CXCR4 in response to the recruitment of overexpressed SDF-1 at ischemia stroke injured foci, and enable endothelial adhesion *via* VLA-4 binding to the upregulated VCAM-1 on the surface of inflamed BMECs. Upon uptake by BMECs, MSCo/miR-132-3p can escape from lysosome through the H_{II} phase transition of 1,2-dioleoyl-*sn*-glycero-3-phosphoethanolamine (DOPE), which is important excipient of the nanovesicles, and then release miR-132-3p to suppress the transcription of the *RASA1* gene and mobilize the downstream RAS/PI3K/AKT signal pathway, which performs anti-apoptosis, oxidative stress alleviation and BBB preservation for ischemia stroke-induced injury treatment.

2. Materials and methods

2.1. *Materials*

miR-132-3p, FAM-miR-132-3p, and Cy3-miR-132-3p were provided by Sangon Biotech Co., Ltd. (Shanghai, China). Hydrogenated soybean phosphatidylcholine (HSPC) was supplied by A. V.T. Pharmaceutical Co., Ltd. (Shanghai, China). 1,2-Dioleoyl-*sn*-

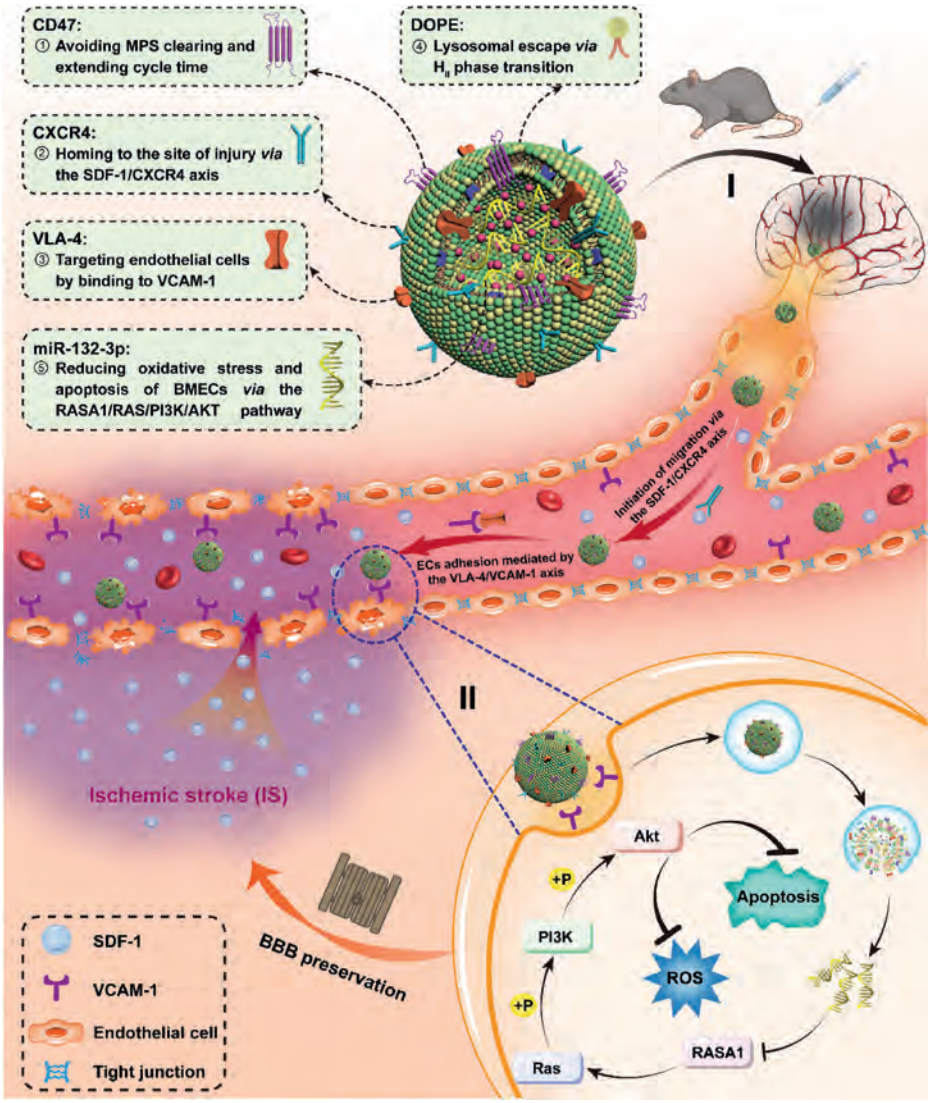

Figure 1 Illustration of the compositions of MSCo/miR-132-3p and its protective effect on BMECs of ischemia stroke. (I) MSCo/miR-132-3p prolongs circulation time after intravenous injection, targets the ischemic cerebrum *via* SDF tropism, and uptake by BMECs through binding to inflammation-upregulated VCAM-1. (II) The escape of MSCo/miR-132-3p from the lysosome under DOPE H_{II} phase transition and the following anti-oxidative stress and anti-apoptotic effects through the RASA1/RAS/PI3K/AKT pathway of BMECs.

glycero-3-phosphoethanolamine (DOPE), cyanine 7-polyethylene glycol 2000-1,2-distearoyl-*sn*-glycero-3-phospho-ethanolamine (Cy7-PEG_{2000}-DSPE) was offered by Xi'an Rui Xi Biotechnology Co., Ltd. (Xian, China). Cholesterol, chlorpromazine (CPZ), and methyl-β-cyclodextrin (MβCD) were purchased from Aladdin Biochemical Technology Co., Ltd. (Shanghai, China). Amiloride (EIPA) was purchased from Macklin Biochemical Co., Ltd. (Shanghai, China).

Agarose was obtained from Biowest (Nuaillé, France). Cell Counting Kit (CCK) was obtained from TransGen Biotech Co., Ltd. (Beijing, China). Reactive Oxygen Species Assay Kit, One Step TUNEL Apoptosis Assay Kit, BeyoBlue™ Coomassie Blue Super Fast Staining Solution, InstantView™ Red Fluorescent DNA Loading Buffer (6 ×), Tris Acetate-EDTA (TAE) buffer, Lyso-Tracker Red, DiO, Dil, TritonX100, RIPA lysis solution, BeyoColor™ Prestained Color Protein Marker, SDS-PAGE Protein Sample Loading Buffer (5 ×), glycine, 2-amino-2-(hydroxymethyl)-1,3-propanediol (Tris) and BeyoECL Plus were purchased from Beyotime Biotechnology (Shanghai, China). FuturePAGE™ (4%−20%, 12 Wells) and MOPS-SDS Running Buffer were acquired from ACE Biotechnology (Changzhou, China). Common protease inhibitors (100 ×) and phosphatase inhibitors (100 ×) were provided by Proteintech Group, Inc. (Wuhan, China).

ProteoExtract Native Membrane protein extraction kit, Evans Blue, FITC-dextran, and PVDF membrane (0.22 μm) were purchased from Merck KGaA (Darmstadt, Germany). Mouse TNF-alpha Recombinant Protein was offered by Thermo Fisher Scientific (Waltham, MA, USA). Recombinant mouse SDF1 protein was obtained from Abcam (Cambridge, MA, USA).

The primary antibodies of CD47 (ab214453), SDF1 (ab155090), GAPDH (ab181602), RAS (ab206969), PI3K (ab191606), ZO1 (ab276131) and CLAUDIN5 (ab131259) were purchased from Abcam; VLA-4 (PB0687) was acquired from Boster Biological Technology (CA, USA); CXCR4 (AF5279), VCAM1 (DF6082) and Goat Anti-Rabbit IgG (H + L) HRP (S0001) were supplied by Affinity Biosciences (Cincinnati, OH, USA); CD31 (AF3628) was obtained from R&D Systems (Minneapolis, MN, USA); RASA1 (12935-1-AP); Goat Anti Rabbit IgG (H&L)-Alexa Fluor 594 (RS3611) and Rabbit Anti Goat IgG (H&L)-Alexa Fluor 488 (RS3218) were purchased from ImmunoWay Biotechnology (Plano, TX, USA); p-PI3K (#4228), AKT (#4691) and p-AKT (#4060) were provided by Cell Signaling Technology (Danvers, MA, USA); Ly6G (65078-1-g) and F4/80 (28463-1-AP) were supplied by Proteintech (Rosemont, IL, USA).

2.2. Extraction of MSC membrane protein

Healthy male SPF-grade C57BL/6J mice (4 weeks old) were purchased from the Animals Core Facility of Nanjing Medical University. All experimental procedures complied with Nanjing Medical University's guidelines on laboratory animals' welfare. The work was approved by the Animal Ethics Committee of Nanjing Medical University. MSCs were isolated from mouse bone marrow. Briefly, mice were sacrificed, soaked in 75% ethanol for 10 min, and separated in an ultra-clean bench to obtain the tibia and femur. Both ends of the tibia and femur were opened, and 1 mL of DMEM complete medium was aspirated to flush out the bone marrow into a Petri dish. The cell suspension was blown, filtered through a 70 μm filter, and centrifuged at 300×*g* (TGL-20M, Xiangyi, China). The precipitate was resuspended with DMEM complete medium and then incubated at 37 °C in a cell culture incubator (Heracell 240i, Thermo Fisher Scientific) containing 5% CO_2.

Surface markers of MSCs were identified by flow cytometry (FACSAria II SORP 18, Becton, Dickinson and Company, USA). MSCs were harvested with approximately 1×10^6 cells in each sample tube. Cells were washed twice with PBS, centrifuged at 300×*g* (Xiangyi) for 5 min, and incubated with 1 μg of antibodies against CD34, CD45, CD44, and CD29 for 30 min at 4 °C away from light. The isotype control was set to exclude false positive results. Finally, the cells were washed twice with PBS, centrifuged at 300×*g* (Xiangyi) for 5 min, and resuspended in 300 μL of buffer for detection.

Membrane proteins were extracted from MSCs using a ProteoExtract Native Membrane protein extraction kit and quantified using a BCA kit. Briefly, MSCs were harvested, washed twice with pre-cooled washing buffer, and centrifuged at 100−300×*g* (Xiangyi) for 10 min at 4 °C. The cell precipitate was resuspended with 2 mL of extraction buffer I and 10 μL of protease inhibitor, incubated for 10 min at 4 °C with gentle stirring, and centrifuged at 16,000×*g* (3-30 KS, Sigma, USA) for 15 min at 4 °C. The supernatant was discarded, 5 μL of protease inhibitor and 1 mL of pre-cooled extraction buffer II were added onwards, and after 30 min of incubation at 4 °C with gentle stirring, the supernatant enriched with membrane proteins was transferred to another tube and stored at −80 °C.

2.3. Determination of membrane protein integration rate

MSCosomes with membrane proteins and phospholipids mass ratios of 1:100, 1:50, and 1:20 were prepared, respectively. The protein content in the supernatant of the lipid suspension after centrifugation at 16,000×*g* (Sigma) for 30 min was measured by the BCA method, and the integration rate of the membrane protein was calculated as in Eq. (1):

$$\text{Membrane protein integration rate } (\%) = (P_0 - P_u) \times 100 \,/\, P_0 \quad (1)$$

P_0 is the initial input of membrane proteins, and P_u is the amount of free membrane proteins in the supernatant after centrifugation.

2.4. Membrane protein distribution and orientation assay of MSCosome

MSC membrane protein amino groups were labeled with a Cy5-NHS probe, and the lipid layer was labeled with the lipid-soluble fluorescent dye DiO. The colocalization of the two was investigated by confocal microscopy (100 × Oil Immersion Objective).

One drop of MSCosome solution was deposited on a glow-discharged carbon-coated copper grid, which was then blocked with 5% (*w*/*w*) bovine serum albumin. For immunogold staining, the samples were incubated with three drops of a 100 μg/mL anti-VLA-4 antibody solution (targeting either the extracellular or intracellular domain of VLA-4) for 1 min. Then, the samples were stained with three drops of 10 nmol/L gold-coupled rabbit IgG secondary antibody solution, followed by washing with 10 drops of distilled water. Finally, the samples were negatively stained with 1% uranyl acetate and were imaged using transmission electron microscopy (JEM-1400Flash, Japan Electron Optics Laboratory, Japan).

2.5. Preparation of MSCo/miR-132-3p

HSPC, DOPE, and cholesterol (5:2:3 mol ratio) were dissolved in ethanol. The solvent was evaporated through a rotary evaporator to form a thin film. Protamine and miR-132-3p were separately dispersed in DEPC water, mixed in a 2:1 M ratio, and incubated for 5 min. Films were hydrated with PBS containing miR-132-3p compressed by protamine through an ultrasonic method and then stirred for 30 min. Membrane proteins were added to lipid suspension and extruded ten times through 800, 400, and 200 nm pore-size cellulose acetate membranes, respectively, to obtain an artificial MSC vesicle solution. After centrifugation at 16,000×*g* (Sigma) for 30 min, the MSCo/miR-132-3p was resuspended by PBS and stored at 4 °C until use.

Blank artificial MSC vesicles (MSCosome) were developed using the same method except for adding miR-132-3p. Plain miR-132-3p-loaded liposome (Lipo/miR-132-3p) was developed using the same method except for adding MSC membrane protein as a control formulation. For DiO and Dil labeling nanovesicles, 20 μL of 100 μmol/L DiO or Dil was dissolved in phospholipid-containing ethanol solution to form the thin film.

2.6. Physicochemical characterization of MSCo/miR-132-3p

Size, PDI, and zeta potential of MSCo/miR-132-3p were measured by dynamic light scattering analysis (Zetasizer Nano ZS90, Malvern, USA). The morphological structure of MSCo/miR-132-3p was observed by transmission electron microscope (Japan Electron Optics Laboratory) after negative staining with uranium acetate.

2.7. Drug loading and release of MSCo/miR-132-3p

The calibration curves were established using FAM-miR-132-3p diluted in PBS buffer (pH 7.4) and acetate buffer (pH 5.0) ranging from 0.008 to 8 μg/mL. MSCo/miR-132-3p was fabricated according to the film dispersion method mentioned above. The free miR-132-3p was separated by centrifugation at 16,000×*g* (Sigma) for 30 min and quantified for concentration based on the calibration curve. The encapsulation rate (EE, %) and drug loading (DL, %) of FAM-miR-132-3p were calculated according to Eqs. (2) and (3):

$$\mathrm{EE}\,(\%) = \left(1 - W_\mathrm{f}\right) \times 100 \,/\, W_\mathrm{t} \quad (2)$$

$$\mathrm{DL}\,(\%) = \left(1 - W_\mathrm{f}\right) \times 100 \,/\, W_\mathrm{m} \quad (3)$$

where W_f, W_t and W_m refer to the mass of the free miR-132-3p, the total input miR-132-3p and the drug delivery system, respectively.

To investigate the release of FAM-miR-132-3p, MSCo/miR-132-3p were dispersed in triplicate in 2 mL of PBS buffer (pH 7.4) and acetate buffer (pH 5.0), respectively. At predetermined time points, 200 μL of sample was taken, and fresh buffer was added at the same volume. The cumulative release of FAM-miR-132-3p was quantified by a full-band multifunctional microplate reader (Infinite 200, Tecan, Switzerland).

2.8. Agarose gel electrophoresis

To determine the optimal compression ratio, protamine and miRNA complexes were prepared at varying molar ratios (0:1, 0.4:1, 0.8:1, 1:1, 1.2:1, 1.6:1, and 2:1 of protamine to miRNA) followed by 5-min incubation at 4 °C. The red fluorescent loading buffer was added to the complexes, and 10 μL of the mixture containing 200 ng miRNA was loaded into a 2% agarose gel. The gel was electrophoresed (100 V, 20 min) in a multifunctional horizontal electrophoresis tank (HE-120, Tanon, China) and exposed to the Multifunctional Gel Image Analysis System (1600 Series, Tanon).

To assess the stability of miRNA in vehicles, naked miR-132-3p and MSCo/miR-132-3p were suspended in PBS containing 10% FBS and 0.25% RNase for 0, 1, 2, 4, 8, and 12 h at 37 °C. The samples were collected and electrophoresed.

2.9. Storage and serum stability of MSCo/miR-132-3p

MSCo/miR-132-3p was suspended in PBS alone or PBS containing 10% FBS at the concentration of 0.25 mg/mL and stored at 4 or 37 °C. The hydrodynamic diameter and PDI were monitored over one week by dynamic light scattering analysis.

2.10. Establishment of the inflammatory injury cell model

The bEnd.3 (ATCC, USA) cell line was cultured in Dulbecco's modified Eagle's medium (DMEM) (Thermo Fisher Scientific) containing 10% FBS (Biological Industries, Israel) and 1% Penicillin/Streptomycin (Thermo Fisher Scientific). bEnd.3 cells with logarithmic growth were inoculated on slides at a density of 2×10^4 cells in 12-well plates. After 24 h of culture, cells were stimulated with 10, 50, and 100 ng/mL TNF-α diluted in DMEM. After fixation with 4% (*w*/*v*) paraformaldehyde (PFA) for 10 min and incubation at room temperature for 1 h, the cells were incubated with VCAM-1 antibody at 4 °C overnight and goat anti-rabbit IgG (H&L)−Alexa Fluor 594 secondary antibody for 1 h at room temperature. The surface expression of VCAM-1 on bEnd.3 cells was observed under a confocal laser microscope (CLSM) (LSM800, Zeiss, Germany). To investigate the appropriate stimulation time, bEnd.3 cells were incubated with 100 ng/mL TNF-α for 0, 2, 4, 6, 8, and 12 h, and the expression of VCAM-1 was observed.

2.11. Cellular uptake of MSCo/miR-132-3p

A total of 2×10^4 bEnd.3 cells were seeded in 18 mm glass culture plates (Citotest, China), stimulated with 100 ng/mL TNF-α for 12 h, and then treated with 0.1, 0.2 and 0.4 mg/mL DiO-labeled MSCo/miR-132-3p and Lipo/miR-132-3p for 6 h, respectively. After three cycles of washing with PBS and staining of nuclei with Hoechst, the samples were observed by a fluorescent microscope (DMi8, Leica, Germany).

To investigate the endocytosis mechanism of MSCo/miR-132-3p, 1×10^5 bEnd.3 cells were cultured in 6-well plates and pretreated with CPZ (10 μg/mL), MβCD (10 mmol/L), and EIPA (0.5 mmol/L) for 0.5 h, using the inhibitor-free group as a control. Then, the cells were incubated with 0.25 mg/mL DiO-labeled MSCo/miR-132-3p for 4 h. The fluorescence of each group of 1×10^4 cells was detected by flow cytometry (Becton, Dickinson and Company).

2.12. Lysosomal escape assay

The bEnd.3 cells were seeded in 12-well chamber slides at a density of 2×10^4 cells/well and treated with 100 ng/mL TNF-α for 12 h. Following a 24-h incubation, media was replaced with fresh media resuspended with 0.25 mg/mL FAM-miR-132-3p-

loaded vesicles with or without DOPE in the composition. At the time points of 1, 2, 4, 8, and 12 h, cellular lysosomes were stained with Lyso-Tracker Red, and nuclei were stained with Hoechst. Colocalization of the vesicles and lysosomes was imaged on a CLSM (Zeiss).

2.13. *In vitro transwell migration assay*

To evaluate vesicle tropism for SDF1, the transwell chambers (Corning, USA) were used to establish a monolayer model. Briefly, the bEnd.3 cells were seeded at a density of 5×10^4 in the 24-well transwell upper chamber with a pore diameter of 1 μm. The epithelial volt-ohm meter (Millicell-ERS-2, Millipore, USA) was used to measure the transendothelial electrical resistance (TEER) of cell monolayers seven days later to check for the formation of a dense cell monolayer, and the chamber with TEER value higher than 200 $\Omega \cdot cm^2$ was selected for the experiment. Then, the cells were treated with 100 ng/mL TNF-α for 12 h, and DiO-labeled MSCo/miR-132-3p and Lipo/miR-132-3p were added to the upper chambers in a medium volume of 800 μL, and the lower chambers included 200 μL of medium with or without SDF1. After incubation for 6 h at 37 °C, the fluorescence signals in the lower chambers were detected by a microplate reader.

2.14. *Investigation of immune escape and long-circulation capacity*

RAW264.7 (ATCC, USA) cell line was cultured in DMEM (Thermo Fisher Scientific) containing 10% FBS (Biological Industries, Israel) and 1% Penicillin/Streptomycin (Thermo Fisher Scientific). After reaching logarithmic growth, RAW264.7 cells were inoculated in glass slides at a density of 2×10^4 per well and then cultured at 37 °C in 5% CO_2 for 24 h. Then, DiO-labeled MSCo/miR-132-3p and Lipo/miR-132-3p were incubated with RAW264.7 cells for 2, 4, and 6 h, respectively. The cellular uptake was visualized by fluorescence microscopy.

To investigate the *in vivo* long cycling capacity of MSCo/miR-132-3p, DiO-labeled MSCo/miR-132-3p (2.5 mg/kg) was injected intravenously into Sprague−Dawley rats. A blood sample of about 200 μL was taken from the eye socket at predetermined time points (1, 2, 4, 8, 12, 24, and 48 h). The serum was separated by centrifugation at 3000 rpm (Sigma) for 10 min, and the fluorescence signals were detected by a microplate reader (Tecan).

2.15. *Establishment of the tMCAO mice model*

The animal experiments were approved by the Institutional Animal Care and Use Committee of Nanjing Medical University (approval number: 2107008). The transient middle cerebral artery occlusion/reperfusion (tMCAO/R) model was established as follows: Mice (about 20 g) were anesthetized and maintained during surgery. Carefully separate the common carotid artery (CCA), external carotid artery (ECA), and internal carotid artery (ICA) on one side. After ligating the CCA with a slipknot, the ECA was ligated distally, and another slipknot was prepared proximally with a small incision between them. Then, silicone-coated threads at the tip (Pingdingshan Yushun Biotechnology Co., Ltd., China) were inserted from ECA into ICA to block the middle cerebral artery (MCA) blood flow. One hour later, the threads were removed for blood reperfusion. The sham group performed the same anesthesia and artery exposure procedure without suture insertion.

2.16. *Expression of SDF1 in the brain*

Brains of the tMCAO mice were removed after perfusion with PBS, and the ipsilateral and contralateral brains were labeled with SDF1 antibody for Western blot and immunofluorescence analyses, respectively.

2.17. *In vivo targeting and biodistribution assay*

One hour post-reperfusion, Cy7-labeled MSCo/miR-132-3p and Cy7-labeled Lipo/miR-132-3p were administered (each at 2.5 mg/kg) to tMCAO mice *via* tail vein injection. At 2, 6, and 12 h, mice were imaged with the *In Vivo* Imaging System (IVIS) (IVIS Spectrum, Caliper, USA) to assess targeting and biodistribution. After 12 h of injection, the brain, heart, liver, spleen, lung, and kidney were removed and imaged on the IVIS (Caliper), and the quantification was performed by region of interest (ROI) analysis using the Living Image software (Living Image 4.2, Caliper, USA).

2.18. *TTC staining and brain water content analysis*

The mice in each group were sacrificed 48 h after administration. The brain tissues were harvested, frozen at −80 °C for 5 min, and then cut into 1-mm-wide coronal sections. The slices were stained with 1% (*w*/*v*) TTC solution and left at 37 °C for about 20 min until the infarcted region and normal region showed a clear color difference. Images are captured by the camera, and the infarct area was quantified with ImageJ. Furthermore, brain tissues were immersed in the extraction solution (DMSO: ethanol = 1:1) to fully extract the TTC dye, and the absorbance at 485 nm was detected after centrifugation.

The brains from another batch of mice were isolated to determine the brain water content. Briefly, the brains are weighed (wet weight), followed by dehydrating in an oven at 120 °C for 24 h and weighed again (dry weight). The brain water content was calculated based on Eq. (4):

$$\text{The brain water content (\%)} = (\text{Wet weight} - \text{dry weight})/\text{wet weight} \times 100 \quad (4)$$

2.19. *ROS detection*

For *in vitro* detection, bEnd.3 cells were seeded in slides at a density of 2×10^4, stimulated with 100 ng/mL TNF-α for 12 h, and then treated with empty media and naked miR-132-3p, MSCosome, Lipo/miR-132-3p and MSCo/miR-132-3p dispersed in DMEM for 24 h respectively, using normal cells as a negative control. Cells were then probed with DCFH-DA and observed under the fluorescence microscope (DMi8, Leica, Germany).

For *in vivo* detection, mice were randomly assigned to the sham-operated group and tMCAO groups, and the tMCAO groups are as follows: PBS, naked miR-132-3p, MSCosome, Lipo/miR-132-3p, and MSCo/miR-132-3p. After perfusion with PBS and 4% PFA, the brains of mice were removed, dehydrated by sucrose gradient, embedded in optimal cutting temperature compound (OCT), and then sliced into 20-μm sections after −80 °C freezing. The oxidative stress levels in the brains were detected using the DCFH-DA probe. For the detection of lipid peroxidation degradation products, fresh tissue samples were collected from the peri-infarct area, fully homogenized, centrifuged, and MDA content in

the supernatant was determined by ELISA kit (E-BC-K025-M, Elabscience, China).

2.20. Cell apoptosis detection

In the *in vitro* assay, inflammatory injury cell models were constructed using TNF-α and given naked miR-132-3p, MSCosome, Lipo/miR-132-3p, and MSCo/miR-132-3p, diluted with DMEM. The untreated damaged cells and normal cells were used as the positive and negative controls, respectively. After fixation with 4% PFA and membrane rupture with Triton X-100, bEnd.3 cells were incubated with a TUNEL detection solution for 1 h and observed under a microscope (Leica). Another batch of bEnd.3 cells were inoculated in a 96-well plate, and after the same treatment, cell survival was detected using the CCK8 kit.

In the *in vivo* assay, tMCAO/R mice were injected with PBS, naked miR-132-3p, MSCosome, Lipo/miR-132-3p, and MSCo/miR-132-3p at a dose of 2.5 nmol/L miR-132-3p per mouse. Following 48 h of cycling, the brains of mice were removed after cardiac perfusion with PBS and 4% PFA. The brain tissues were dehydrated and embedded, sectioned into 20-μm slices using a microtome cryostat (CM3050, Leica, Germany), and finally, the apoptotic cells were stained with a TUNEL detection solution.

2.21. Assessment of BBB permeability

An *in vitro* BBB injury model was established as follows: The bEnd.3 cells (5×10^4 cells/well) were implanted into the 24-well transwell upper chamber for 7 days to form an endothelial barrier. Afterward, cells were successively exposed to TNF-α and different formulations (empty media, naked miR-132-3p, MSCosome, Lipo/miR-132-3p, and MSCo/miR-132-3p), with normal cells as a negative control. Then, FITC-dextran (10 kDa, 1 mg/mL) was added into the upper chamber. After 4 h co-culture, the flux of FITC-dextran across monolayer was used to measure the paracellular permeability. The fluorescence in the lower chamber was measured by a fluorescent microplate reader (Tecan).

Evans blue staining was applied to evaluate the BBB permeability *in vivo*. Briefly, after treatment with different formulations (PBS, naked miR-132-3p, MSCosome, Lipo/miR-132-3p, and MSCo/miR-132-3p) for 48 h, the tMCAO mice were injected with 4% Evans blue (4 mL/kg) and transcardially perfused with PBS and 4% PFA. After being sacrificed, the mouse brains were sliced into the 1-mm-thick coronal sections and photographed with a camera. Furthermore, the ischemic hemispheres were homogenized in formamide to dissolve the dye. After centrifugation, the absorbance value of the supernatant at 620 nm was measured by a microplate reader (Tecan) to determine the amount of extravasated dye.

For the detection of the infiltration of immune cells in the brain, the formulations were injected 6 h after ischemia−reperfusion and administered every other day for 5 days. Mice were euthanized on Day 5. Following transcardial perfusion with PBS to remove blood-derived immune cells, neutrophils and macrophages in the ischemic brain hemisphere were labeled with anti-Ly6G and anti-F4/80 antibodies, respectively.

2.22. BMECs and vascular staining

tMCAO/R mice were given different formulations as above, with the sham-operated mice serving as controls. After 48 h, the brains of mice were removed, fixed with 4% PFA for 4 h, dehydrated with 10%, 20%, and 30% sucrose at 4 °C for 24 h, and sectioned into 30-μm frozen coronal slices. Then, the slices were incubated with VCAM-1 antibody (1:100), CD31 antibody (10 μg/mL), and Alexa Fluor 488 conjugated Rabbit Anti Goat secondary antibody (1:1000). The vessel staining was visualized by CLSM (Zeiss). The vessel length in the field was quantified using the Image J software (National Institutes of Health, USA).

Dil-labeled MSCo/miR-132-3p was injected intravenously into mice to observe the colocalization of MSCo/miR-132-3p with BMECs and blood vessels. The brains of mice were cut into 30-μm slices, and after fluorescent tagging of the vascular marker CD31 with antibodies, the brain sections were scanned and imaged using CLSM (Zeiss).

2.23. Measurement of cerebral blood flow

The cerebral blood flow (CBF) of mice in each group was measured by the SIM BFI HR PRO System (Simopto, China). Specifically, after administration of different formulations for 48 h, mice were anesthetized and placed on the stereotaxic apparatus. The skin on the head was cross-cut to expose the whole skull. The laser scatter blood flow imaging system was applied to scan the intact skull for approximately 1 min. The relative CBF (rCBF) was calculated based on Eq. (5):

$$\text{rCBF}\ (\%) = \text{CBF of ipsilateral side/CBF of contralateral side} \times 100 \quad (5)$$

2.24. Comparison of artificial vesicles and natural vesicles

Natural MSC extracellular vesicles were extracted by differential centrifugation. EX-depleted MSC culture medium was collected and centrifuged at $300\times g$ (Sigma) for 5 min, $2000\times g$ (Sigma) for 10 min, and $10{,}000\times g$ (Sigma) for 30 min to discard the sediments. The supernatant is filtered through a 0.22 μm filter, ultracentrifuged at $100{,}000\times g$ (OptimaL-100XP, Beckman, USA) for 90 min at 4 °C, and washed once with PBS. The precipitate was resuspended with 200 μL PBS and stored at −80 °C for long periods of time. The size and morphology of natural vesicles were characterized by DLS (Malvern) and TEM (Japan Electron Optics Laboratory).

tMCAO mice were given natural MSC extracellular vesicles and artificial vesicles every other day, and the therapeutic effect was evaluated after continuous administration for 1 week. Neurological function scores and TTC staining were used to investigate the efficacy of both.

2.25. Investigation of MSCo/miR-132-3p efficacy

The therapeutic potential of MSCo/miR-132-3p was examined in tMCAO mice by intravenous administration of the aforementioned preparations every other day for 7 days. The survival time, body weight changes, and behavioral parameters were recorded for all groups of mice. After being sacrificed, the brains of the mice were removed for hematoxylin−eosin (H&E) staining to visualize the infarct area.

For behavioral assessment, we focused on neurological function scores, the balance beam test, and the muscle strength test. A well-established five-point scale methodology was used to evaluate the neurological function with a rating scale: 4 = spontaneous circling, 3 = circling to the left by pulling the

tail, 2 = weakened grip strength of the left forepaw, 1 = failure to extent left forepaw, and 0 = no deficit. In the balance beam test, mice were placed in the middle of the bar and allowed to crawl freely. The test was completed when the mice fell off the bar, and the dwell time was recorded, measured for a maximum of 180 s, and repeated 3 times with 5-min intervals. In the muscle strength test, the time the mice spent gripping the wire rope was recorded, with the longest test time not exceeding 180 s.

2.26. SDS gel and Western blot detection

The protein expression profiles of total protein, membrane protein, MSCosome, and bare liposome were analyzed using SDS-PAGE. After protein quantification by the BCA method, each group was diluted with RIPA lysate, mixed with 5X loading buffer, heated at 100 °C for 10 min, and loaded onto a 4%−20% Bis-Tris protein gel in a volume of 20 μL containing 60 μg of protein per well. Staining was performed with the Coomassie blue super fast staining solution.

For Western-blot analysis, pellets and brain tissue were lysed with RIPA, centrifuged at 12,000×*g* for 20 min, and the proteins were collected and quantified. After being separated by SDS-PAGE, proteins were transferred onto the PVDF membrane. The membranes were incubated under agitation at room temperature with 5% nonfat milk in 0.1% Tween 20 in TBS (TBST) for 1 h and incubated with primary antibodies against CD47 (1:1000), CXCR4 (1:500), VLA-4 (1:1000), anti-RASA1 (1:1000), anti-RAS (1:1000), anti-PI3K (1:1000), anti-p-PI3K (1:1000), anti-AKT (1:1000), anti-p-AKT (1:2000), anti-ZO1 (1:1000), anti-CLAUDIN5 (1:1000) and anti-GAPDH (1:10000) in agitation at 4 °C overnight, followed by HRP-conjugated IgG secondary antibody (1:5000). The bands were soaked with ECL luminescent solution and exposed in the Fully Automated Chemiluminescence Image Analysis System (4600 Series, Tanon).

2.27. In vivo preliminary biocompatibility evaluation

Healthy C57BL/6 mice (about 20 g) were randomly divided into three groups and administrated with PBS, MSCosome (2.5 mg/kg), and MSCo/miR-132-3p (2.5 mg/kg), respectively, which were injected into the tail vein every other day for 14 days. The body weight changes were recorded, and then the mice were sacrificed. Major organs (heart, liver, spleen, lung, kidney, and brain) were harvested and stained with H&E, and the blood was analyzed for routine biochemical indices and blood cells.

2.28. Statistical analysis

Data were presented as the means ± standard deviation (SD). Statistical analysis of differences between the experimental groups was performed using multiple Student's *t*-tests and one-way ANOVA. Differences were considered statistically significant when $P < 0.05$ ($^{*}P < 0.05$, $^{**}P < 0.01$, and $^{***}P < 0.001$).

3. Results

3.1. Preparation and characterization of MSCo/miR-132-3p

The preparation of MSCo/miR-132-3p is described in Fig. 2A. Here, we applied a membrane protein integration method to prepare artificial MSC extracellular vesicles, which is different from the traditional cell membrane camouflage method. This method combined the advantages of both "top-down" and bottom-up: techniques with the convenience of obtaining highly complex bionic surfaces in one step, the flexibility of prescription adjustment, and the tunability of physicochemical parameters[36]. Firstly, bone marrow MSCs were extracted from mice using an improved whole-bone marrow apposition method and were purified and expanded *in vitro*. It was observed that after a period of culture, the cells showed fibroblast-like growth, tending to be long fusiform and irregular polygonal and arranged in swirls (Supporting Information Fig. S1A). The expression of the typical negative markers CD34 and CD45 and the positive markers CD29 and CD44 on the surface of the MSCs was identified using flow cytometry, yielding a high percentage of MSCs of more than 95% (Fig. S1B and S1C). To screen the optimal ratio of membrane proteins to phospholipids in the prescription, we fabricated artificial MSCs vesicles (MSCosome) with membrane proteins and phospholipids mass ratios of 0:1, 1:100, 1:50, and 1:20, respectively. The integration rate of membrane proteins was determined by the Bicinchoninic Acid (BCA) assay, which dropped with the addition of protein content and was able to maintain above 95% at a ratio of 1:50 (Fig. 2B, Supporting Information Table S1). Furthermore, the protein-phospholipid ratio had no significant effect on the particle size of MSCosome, and the polydispersity index (PDI) increased slightly compared with that of blank liposomes yet stayed below 0.25, indicating a homogeneous particle size and a concentrated size distribution (Fig. 2C and D, Table S1). The zeta potential declined with the growing proportion of proteins, which suggested that the membrane proteins were successfully incorporated into the phospholipid bilayer on the other side (Fig. 2E, Table S1). Based on these results, the ratio of 1:50 was chosen in the final prescription, which has a high membrane protein content while maintaining a good protein integration rate. Transmission electron microscopy (TEM) images showed that MSCosome had a uniform particle size distribution while presenting a homogeneous bilayer structure (Supporting Information Fig. S2A and S2B). The function of the artificial vesicles depends on the integrated membrane proteins. It was shown that MSCosome had an expression profile similar to that of MSC membrane proteins, and Western blot proved that the critical membrane proteins of MSCs (CD47, CXCR4, and VLA-4) were successfully transferred to the surface of MSCosome (Fig. 2F and G). The distribution of membrane proteins in the bilayer was detected by fluorescence labeling. Specifically, proteins were labeled with the Cy5-NHS probe, and vesicles were labeled with the DiO fluorescent dye. The colocalization results showed that the protein was successfully integrated into the liposomes and showed a uniform distribution (Supporting Information Fig. S3). The right membrane protein orientation of MSCosome for molecular interactions was further examined. VLA-4 is a specific biomarker of MSCs with both an extracellular domain and intracellular domain, and immunogold staining experiments targeting different domains of VLA-4 were studied. As shown in Supporting Information Fig. S4, TEM images confirmed the presence of the VLA-4 extracellular domain on the outer surface of the MSCosome, but no significant staining of the VLA-4 intracellular domain was observed, which indicated the correct right-side-out membrane protein orientation on the surface of the artificial MSC extracellular vesicles.

To encapsulate miR-132-3p into MSCosome, we first compressed miR-132-3p with protamine, a naturally cationic protein that can efficiently concentrate mRNA to form polyplex[37]. The

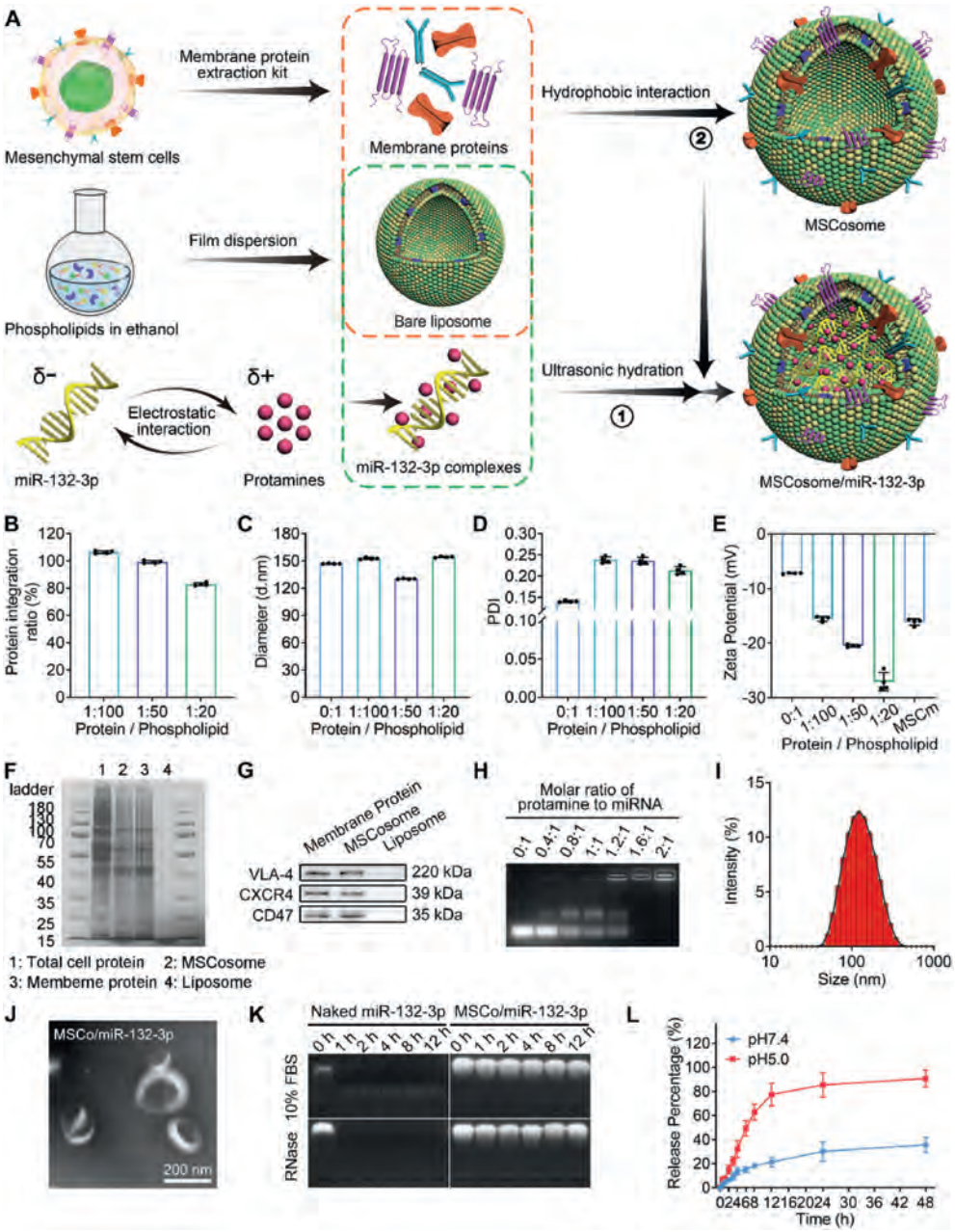

Figure 2 Preparation and characterization of MSCo/miR-132-3p. (A) Preparation of MSCosome and MSCo/miR-132-3p. (B−E) Membrane protein integration rate, diameter, PDI, and zeta potential of MSCosome at different phospholipid to membrane protein ratios ($n = 4$). MSCm: MSC membrane. (F, G) SDS-PAGE and Western-blot analysis of MSCosome. (H) Electrophorogram of protamine/miRNA complexes with different molar ratios. (I, J) Size distribution and TEM image of MSCo/miR-132-3p. Scale bar = 200 nm. (K) Stability of MSCo/miR-132-3p in PBS with 10% FBS and 0.25% RNase detected by agarose electrophoresis. (L) Drug release profiles of MSCo/miR-132-3p under different pH conditions ($n = 3$). Data are presented as mean ± SD.

electrophoresis results indicated great compression efficiency when the molar ratio of protamine to miR-132-3p reached 2:1 (Fig. 2H). MSCo/miR-132-3p prepared in this ratio possessed a particle size of around 120 nm and an even spherical vesicular form with a lipid bilayer (Fig. 2I and J). The physical characterization of MSCosome and MSCo/miR-132-3p were summarized in Supporting Information Fig. S5A−S5C and Table S2. The small particle size and negative surface potential favored the avoidance of MPS clearance and non-specific conjugation to serum proteins, obviating accumulation in the capillaries of the spleen, liver, and lungs and lengthening the circulation time. The encapsulation rate and drug loading of miR-132-3p were 91.07 ± 0.81% and 19.79 ± 0.14%, respectively (Supporting Information Table S3). In addition, the supernatant of MSCo/miR-132-3p was harvested after high-speed centrifugation and electrophoresed in 1.5% agarose gel. There was almost no detection of free RNA, further indicating that the vast majority of miR-132-3p was packaged into the artificial vesicles (Fig. S5D). To validate the protective effect of the miRNA, naked miR-132-3p and MSCo/miR-132-3p were dispersed in PBS containing 10% FBS and 0.25% RNase and

collected at predetermined time points for electrophoresis. In contrast to naked miR-132-3p rapid degradation, MSCo/miR-132-3p could show bright RNA bands even at 12 h, which implied that the lipid vesicles could shield miRNAs from various components in the blood and RNase (Fig. 2K). Furthermore, FAM fluorescent labeled miR-132-3p was used to examine the release behavior under different pH conditions. MSCo/miR-132-3p artificial nanovesicles cleaved faster under acidic conditions, releasing up to 90% of FAM-labeled miR-132-3p *versus* only about 35% under neutral conditions (Fig. 2L), and the release kinetic parameters are presented in Supporting Information Table S4. It is speculated that this might be owing to the inclusion of the pH-sensitive DOPE in the component of MSCo/miR-132-3p, which is stable under neutral conditions and transforms to the inverted Hexagonal II (H_{II}) phase under acidic conditions, fostering the fusion of lipid membranes with endosomal membranes to enable the lysosomal escape of miRNAs[38,39]. The existence of DOPE made the vesicles destabilized under acidic conditions and more prone to leakage. In addition, MSCo/miR-132-3p were stable in PBS or PBS containing 10% FBS for more than one week, with no significant changes in particle size or PDI (Supporting Information Fig. S6A and S6B), and homogeneous with no visible precipitation (Fig. S6C). BCA detection showed that the protein content in vesicles did not decrease significantly after one week of storage at 4 °C (Fig. S6D).

3.2. Targeting and uptake behavior of MSCo/miR-132-3p

VLA-4 expressed on the surface of MSCs specifically binds to VCAM-1 on the surface of vascular endothelial cells, leading to MSCs migration to the nearby microvessels and adhesion to the endothelium[40,41]. The inflammatory response is initiated in the acute phase of ischemia stroke and proceeds with the course of injury, whose extent correlates with the severity and prognosis of stroke. To imitate the inflammatory microenvironment in which BMECs are exposed in ischemia stroke, we stimulated bEnd.3 cells with tumor necrosis factor (TNF-α). Immunofluorescence staining revealed that the expression level of VCAM-1 was positively associated with the concentration of TNF-α, and when the concentration reached 100 ng/mL, the fluorescence of VCAM-1 on the surface of bEnd.3 cells was the strongest, which was adopted for the subsequent establishment of the bEnd.3 cell damage model (Supporting Information Fig. S7A and S7B). Besides, bEnd.3 cells were co-incubated with 100 ng/mL TNF-α for 0.5, 2, 4, 6, 8, and 12 h, and a TNF-α incubation time-dependent enhancement of VCAM-1 expression was observed under confocal laser scanning microscope (CLSM), which leveled off after 6 h (Supporting Information Fig. S8A and S8B). The bEnd.3 injury model was then used to validate the *in vitro* targeting of the artificial vesicles. The uptake of MSCo/miR-132-3p by bEnd.3 cells was obviously superior to that of Lipo/miR-132-3p owing to the existence of VLA-4 and showed a concentration-dependent pattern (Fig. 3A and B).

Herein, it was indicated that the secretion of SDF-1 in the ischemia stroke injured hemisphere was much higher than that in the contralateral hemisphere by immunofluorescence staining and Western blot analysis (Fig. 3C and D, Supporting Information Fig. S9), which was consistent with the previous report[31]. To determine if artificial vesicles are recruited to ischemic stroke-injured brain regions through the SDF-1/CXCR4 axis, we conducted an *in vitro* Transwell migration assay (Fig. 3E). It could be seen that the fluorescence intensity of the Lipo/miR-132-3p group was weaker regardless of the presence or absence of SDF-1, whereas that of the MSCo/miR-132-3p group was the strongest in the presence of SDF-1, indicating that the integration of CXCR4 induced the homing of MSCo/miR-132-3p to the ischemic regions enriched with SDF-1 (Fig. 3F).

DOPE can endow the vesicles with the capacity of lysosomal escape. Therefore, we prepared DOPE-containing and DOPE-free MSCo/miR-132-3p and added them to the culture system of bEnd.3 cells. The co-localization of the both and cytosolic lysosomes was visualized at different time points (1, 2, 4, 8, and 12 h). DOPE-deficient MSCo/miR-132-3p exhibited distinct yellow fluorescence after uptake by bEnd.3 cells, which was attributed to the overlap of the green fluorescence of FAM-miR-132-3p with the red fluorescence of Lyso-Tracker. There was no observable separation of the two colors over time, indicating that the lack of DOPE resulted in failed lysosomal escape and rapid RNA degradation. In contrast, the green fluorescence of MSCo/miR-132-3p containing DOPE appeared at 2 h after cellular uptake and was separated clearly at 8 h, implying that a significant portion of MSCo/miR-132-3p had extricated from the lysosome (Fig. 3G). The cellular endocytosis mechanism of MSCo/miR-132-3p was investigated by incubation with the clathrin inhibitor chlorpromazine (CPZ), the caveolae inhibitor methyl-β-cyclodextrin (MβCD), and the macropinocytosis inhibitor 5-(*N*-ethyl-*N*-isopropyl) amiloride (EIPA), and the untreated cells were set as a control. It was shown that all three inhibitors reduced the cellular uptake of MSCo/miR-132-3p, with CPZ standing out, signifying the predominance of the clathrin-dependent endocytosis, which progresses through the lysosome, rendering lysosomal escape ability essential for MSCo/miR-132-3p (Fig. 3H and I).

3.3. Immune evasion and brain targeting of MSCo/miR-132-3p

Intravenously injected exogenous substances undergo a complex biological process preceding their arrival at the treatment site *in vivo*, during which they may be recognized by the MPS and cleared in large quantities. The integrin-associated protein CD47 is a broadly distributed cell-surface glycoprotein first identified in stem cells and ubiquitous in most cells in the body. CD47 combines with the inhibitory receptor signal regulatory protein α (SIRPα) found on the surface of neutrophils, monocytes, monocyte-derived cells, etc., and acts as a self-marker to send a "don't eat me" signal, preventing cells from being nonspecifically cleared[42,43]. It was proved that CD47 was superficially expressed in the artificial MSCs extracellular vesicles by Western blot (Fig. 2G). To check whether it is possible to evade immunosurveillance, we incubated MSCo/miR-132-3p with macrophages for different times *in vitro* using Lipo/miR-132-3p as a control. It was observed that MSCo/miR-132-3p had little intra-macrophage accumulation, whereas the cellular fluorescence within Lipo/miR-132-3p turned to be exceedingly luminous over time, suggesting the MSCo/miR-132-3p avoided being recognized and scavenged by macrophages (Fig. 4A and B). In order to examine if the artificial extracellular vesicles possessed *in vivo* long circulation, the SD rat pharmacokinetic assay was studied, in which DiO-labeled Lipo/miR-132-3p and MSCo/miR-132-3p were injected into rats by tail vein, and orbital blood was harvested to determine the fluorescence intensity, respectively. In contrast to Lipo/miR-132-3p, MSCo/miR-132-3p had a significantly longer half-life ($t_{1/2} \approx 48$ h), affording a prerequisite for the subsequent migration to brain capillary endothelial cells at the site of ischemia stroke injury (Fig. 4C, Supporting Information Table S5).

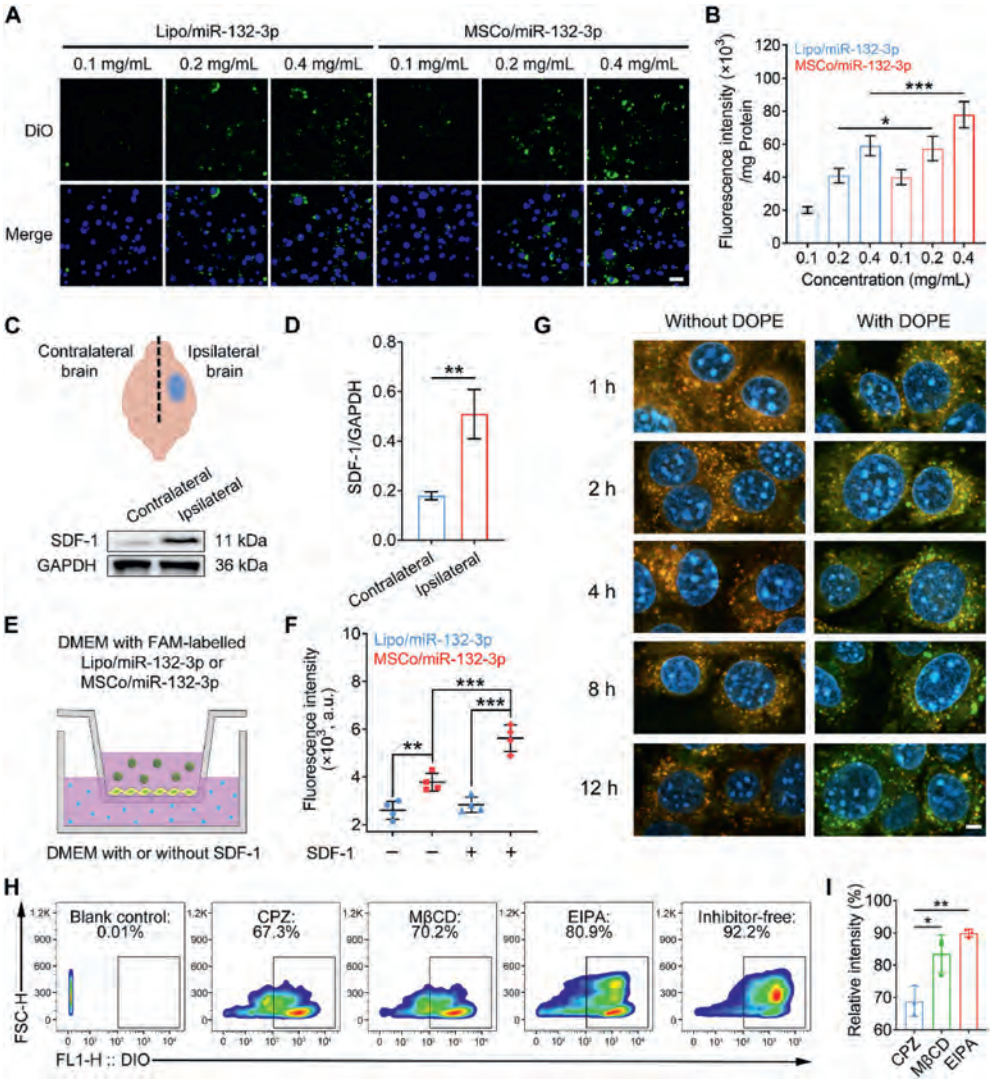

Figure 3 Cellular evaluation of MSCo/miR-132-3p. (A, B) Fluorescent images and quantification of bEnd.3 after incubation with different concentrations of Lipo/miR-132-3p and MSCo/miR-132-3p ($n = 3$). Green: DiO-labeled vesicles; blue: nuclei. Scale bar = 50 μm. (C, D) Western-blot analysis and normalization of expression of SDF-1 in the ipsilateral and contralateral brain after ischemic stroke ($n = 3$). (E) Diagram of the *in vitro* monolayer model to evaluate the homing of MSCo/miR-132-3p to SDF-1. (F) The fluorescence intensity of DiO-labeled vesicles in the basal chamber of the transwell at 6 h ($n = 3$). (G) Representative colocalization images of DOPE-containing and DOPE-free vesicles with lysosomes. Green: FAM-miR-132-3p; red: Lyso-Tracker; blue: nuclei. Scale bar = 5 μm. (H, I) Flow cytometry scatterplot and fluorescence quantification of the endothelium endocytosis of MSCo/miR-132-3p probed by different inhibitors ($n = 3$). Data are presented as mean ± SD. $^*P < 0.05$, $^{**}P < 0.01$, $^{***}P < 0.001$.

Furthermore, the *in vivo* bio-distribution of Cy7 fluorescence labeled MSCo/miR-132-3p of tMCAO mice was investigated by real-time fluorescence imaging. As illustrated in Fig. 4D and E, the fluorescence in the brain of mice in the Sham and plain Lipo/miR-132-3p group declined with time and became very weak after 12 h, while the MSCo/miR-132-3p group maintained robust fluorescence, which benefited from the targeting to the ischemia stroke injured brain regions and the long-circulation competence of the MSCo/miR-132-3p. Major organs (brain, heart, liver, spleen, lungs, and kidneys) of the mice were isolated after 12 h. The results disclosed that the fluorescence accumulation of MSCo/miR-132-3p group was much higher than the other two in the brain, and there was no apparent discrepancy between the allocation of Lipo/miR-132-3p in the left and right hemispheres given the lack of targeting to the site of injury, unlike MSCo/miR-132-3p that could selectively aggregate in the damaged brain side (Fig. 4F−H, Supporting Information Fig. S10A and S10B). Scanning of brain sections of tMCAO mice injected with Dil-labeled Lipo/miR-132-3p and MSCo/miR-132-3p authenticated the same findings (Supporting Information Fig. S11). In addition, the colocalization of the intracerebral blood vessels stained with CD31 antibody and Dil-labeled Lipo/miR-132-3p and MSCo/miR-132-3p were observed by CLSM. The results showed that MSCo/miR-132-3p could be more remarkably enriched in ischemia-injured cerebral vessels compared to Lipo/miR-132-3p (Fig. 4I). In order to further verify the targeting mechanism, we investigated the colocalization of Lipo/miR-132-3p and MSCo/miR-132-3p with VCAM-1 in the infarct brain area. The results

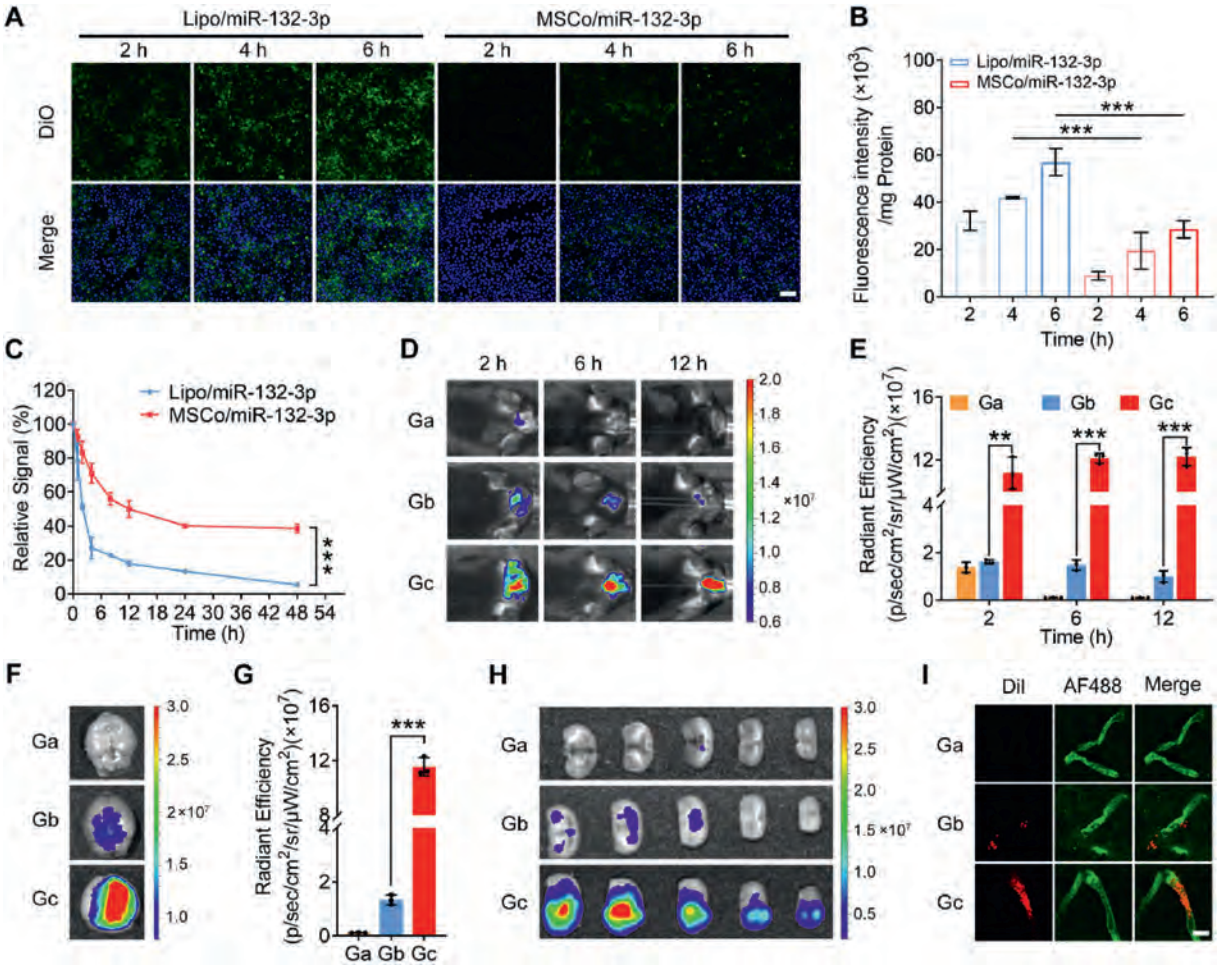

Figure 4 Immune evasion and brain targeting of MSCo/miR-132-3p. (A, B) Fluorescence images and quantification of Lipo/miR-132-3p and MSCo/miR-132-3p uptake by RAW264.7 cells ($n = 3$). Green: DiO labeled vesicles; blue: nuclei. Scale bar = 50 μm. (C) Blood retention of DiO-labeled artificial vesicles in SD rats after a single intravenous injection ($n = 3$). (D, E) *In vivo* imaging and fluorescence quantification of tMCAO mice at different time points after injection of Cy7 labeled artificial vesicles ($n = 3$). Group: Ga: Sham; Gb: Lipo/miR-132-3p; Gc: MSCo/miR-132-3p. (F–H) *Ex vivo* imaging, quantification of isolated brain tissue, and imaging of brain sections of tMCAO mice 12 h after injection of Cy7 labeled artificial vesicles ($n = 3$). (I) Microscopic detection of Lipo/miR-132-3p and MSCo/miR-132-3p in the cerebral vasculature marked with CD31 antibody. Red: Dil-labeled vesicles; green: Alexa Fluor 488 conjugated to CD31 antibody. Scale bar = 10 μm. Data are presented as mean ± SD. $^{**}P < 0.01$, $^{***}P < 0.001$.

showed that compared with Lipo/miR-132-3p, MSCo/miR-132-3p could significantly enrich the VCAM-1 expression region through surface VLA-4 protein (Supporting Information Fig. S12).

3.4. MSCo/miR-132-3p attenuated oxidative stress and apoptosis of BMECs to preserve BBB function

To ascertain how MSCo/miR-132-3p exerts curative effects on BMECs, TNF-α stimulated bEnd.3 cells were used as an *in vitro* model to evaluate the oxidative stress and apoptosis after treatment by various formulations. It was noted that the intracellular ROS levels of the naked miR-132-3p group were almost identical to those of the unadministered control group, which was caused by the rapid degradation of miR-132-3p, losing the shield of the lipid bilayer. Despite the ability to target bEnd.3, the absence of the critically therapeutic miR-132-3p restricted the mitigation of ROS levels of the blank MSCosome group. MSCo/miR-132-3p maximally diminished intracellular oxidative stress levels in BMECs *versus* Lipo/miR-132-3p, which was deficient in the BMECs target (Fig. 5A and B). The apoptosis of bEnd.3 was further examined using a TUNEL assay kit, and MSCo/miR-132-3p treatment minimized the level of apoptosis among all these groups (Fig. 5C). In addition, it was indicated that MSCo/miR-132-3p restored the cell viability to approximately 87% than merely ∼60% of the naked miR-132-3p groups by CCK8 assay (Supporting Information Fig. S13A). Since it was identified that MSCo/miR-132-3p had a curative effect on BMECs, the pivotal ingredients of BBB, we studied the BBB protection of MSCo/miR-132-3p *in vitro* and *in vivo*, respectively. The flux of FITC-dextran penetration across TNF-α-stimulated bEnd.3 monolayer was calculated to determine the *in vitro* BBB permeability, which was significantly decreased after MSCo/miR-132-3p treatment among these groups (Fig. S13B).

Next, we investigated the protective effects of MSCo/miR-132-3p on the BBB and cerebral vasculature *in vivo,* and the timelines of the specific experiments are presented in Supporting Information Fig. S14A. First, the permeability of the BBB was examined by extravasation of Evans blue dye. It was shown that the diffusion

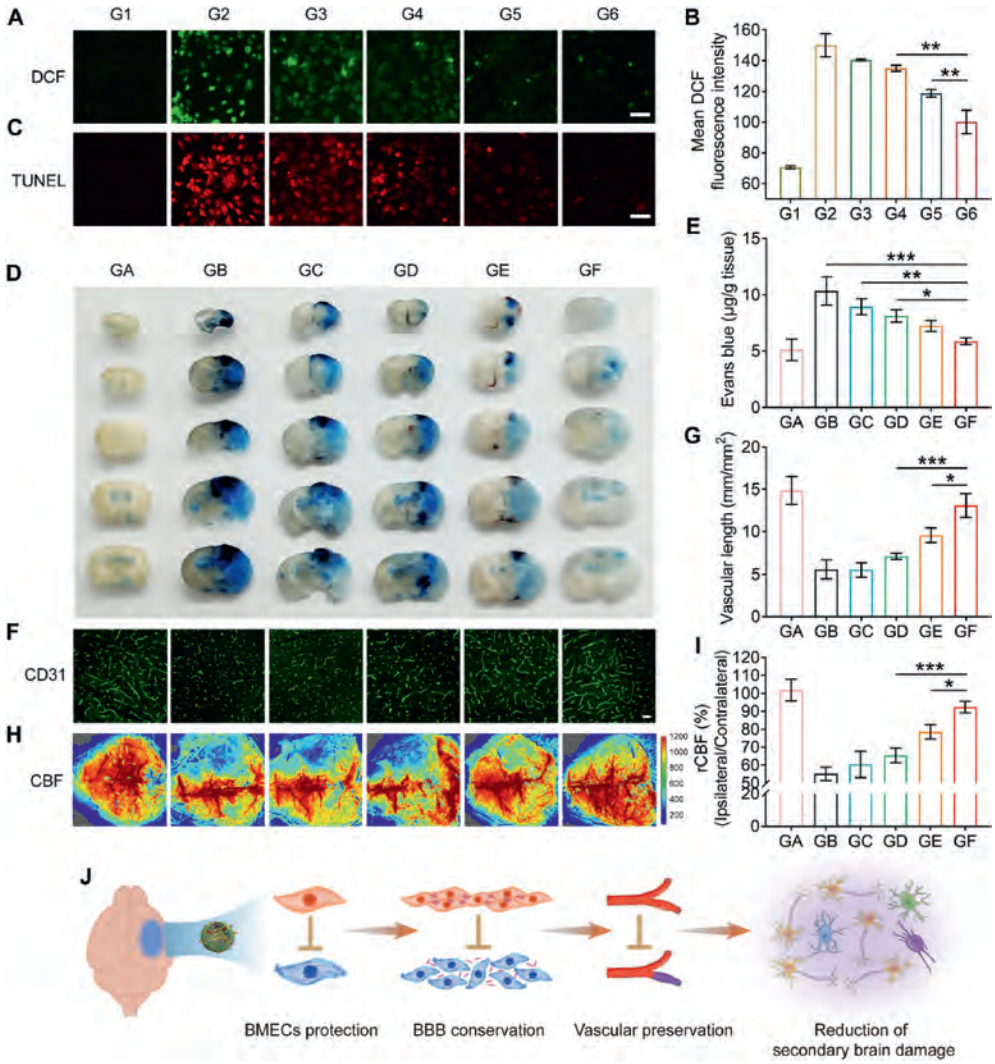

Figure 5 Protective effects of MSCo/miR-132-3p on BMECs and the BBB. (A, B) Representative images of ROS staining of bEnd.3 and quantification by flow cytometry ($n = 3$). Scale bar = 50 μm. Group: G1: Control; G2: Medium; G3: Naked miR-132-3p; G4: MSCosome; G5: Lipo/miR-132-3p; G6: MSCo/miR-132-3p. (C) Representative images of apoptosis staining of bEnd.3. Scale bar = 50 μm. (D, E) Photographs and quantification of the Evans blue extravasation in brain slices of tMCAO mice ($n = 3$). Group: GA: Sham; GB: PBS; GC: Naked miR-132-3p; GD: MSCosome; GE: Lipo/miR-132-3p; GF: MSCo/miR-132-3p. (F, G) Representative images and density quantification of CD31-positive microvessels in the infarct region of tMCAO mice ($n = 3$). Scale bar = 50 μm. (H, I) rCBF images and quantification ($n = 3$). (J) Diagram of the effects of MSCo/miR-132-3p on BMECs and BBB. Data are presented as mean ± SD. $^*P < 0.05$, $^{**}P < 0.01$, $^{***}P < 0.001$.

of the dye was the greatest in the brain tissue of tMCAO model mice with severe BBB damage and much less in the brain of mice treated by the MSCo/miR-132-3p group that were able to protect the BBB (Fig. 5D and E). BBB permeability is positively correlated with the degree of vascular damage, implying a reduction in the number of intact vessels and a subsequent reduction in cerebral blood flow. The preservation of intracerebral blood vessels by different treatments was examined by staining the vascular marker CD31 and quantifying the length of the observed vessels. Untreated tMCAO mice had the worst cerebrovascular damage, with rarely intact long blood vessels, coinciding with those subjected to naked miR-132-3p, which was ameliorated by Lipo/miR-132-3p but not as much as MSCo/miR-132-3p due to the non-selectivity for BMECs (Fig. 5F and G). The blood flow in the brain of tMCAO mice was monitored through laser speckle contrast imaging, which was much lower in the ischemic hemisphere than in the contralateral hemisphere. Among these groups, MSCo/miR-132-3p provided the utmost conservation of the vasculatures in the ischemic hemisphere, maintaining a majority of normal blood flow (Fig. 5H and I). The paradigm of MSCo/miR-132-3p targeted repair of BBB was presented in Fig. 5J. MSCo/miR-132-3p selectively protected BMECs and maintained their connectivity, thereby decreasing the permeability of BBB, maintaining normal cerebral blood flow, and reducing secondary damage due to the entry of substances from the bloodstream into the brain and ischemia-induced oxygen and nutrient deficiencies.

3.5. MSCo/miR-132-3p reduced cerebral ischemia–reperfusion injury, restored neurological function, and prolonged survival time of MCAO mice

The BBB plays a pivotal role in the exchange of substances between the brain and the external circulation. Therefore, alleviating BBB impairment during the acute phase of ischemia stroke

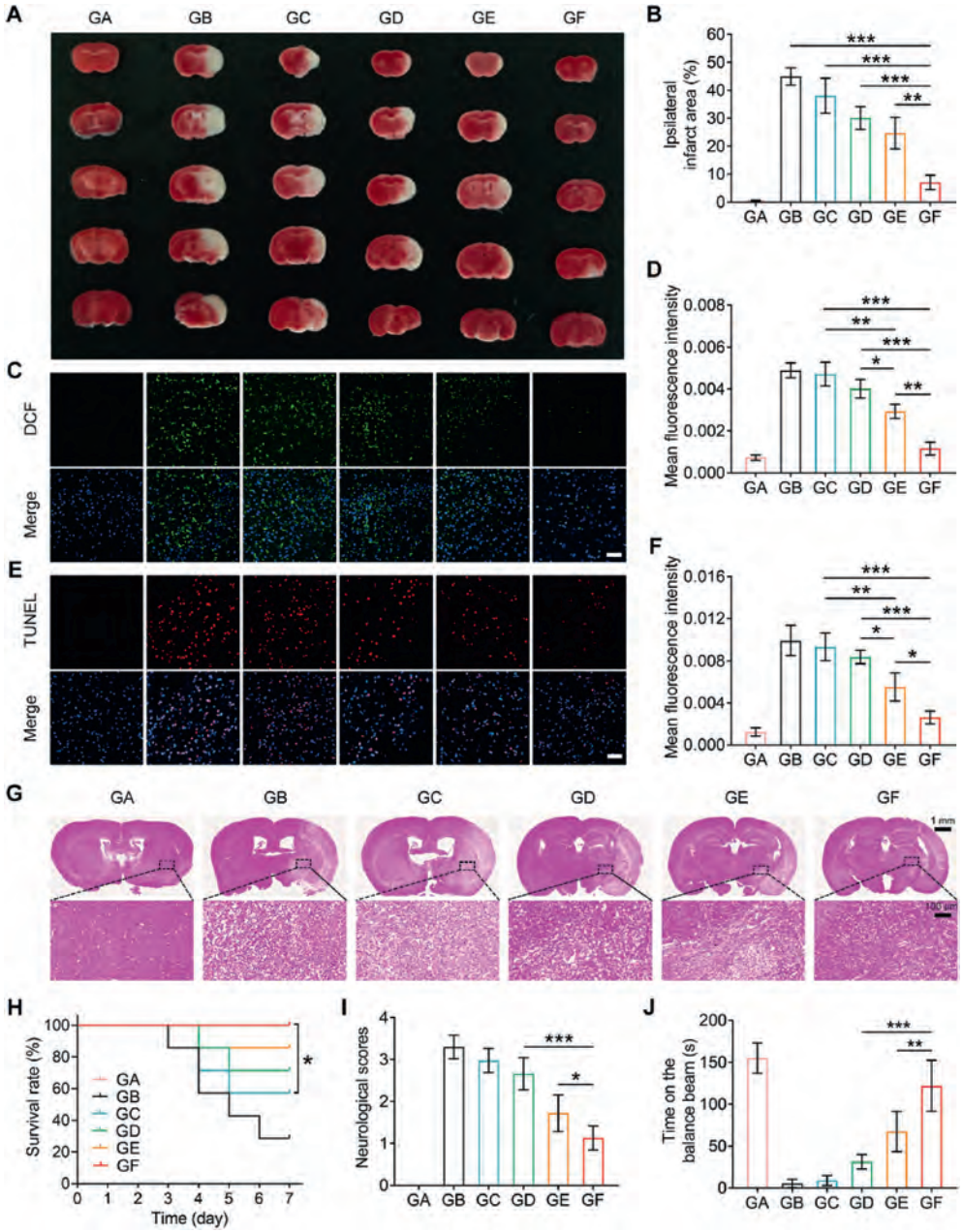

Figure 6 Therapeutic efficacy of MSCo/miR-132-3p for ischemic stroke. (A, B) TTC staining images and quantification of brain slices of tMCAO mice ($n = 3$). Group: GA: Sham; GB: PBS; GC: Naked miR-132-3p; GD: MSCosome; GE: Lipo/miR-132-3p; GF: MSCo/miR-132-3p. (C−F) Representative images and MFI of ROS and apoptosis staining of the ischemic penumbra ($n = 3$). Scale bar, 50 μm. (G) Pathological examination of cerebral sections. Sections framed by the rectangle are magnified. Scale bar, 1 mm (top) & 100 μm (bottom). (H−J) Survival rate, neurological scores, and time on the balance beam of mice treated with different formulations ($n = 7$). Data are presented as mean ± SD. $^{*}P < 0.05$, $^{**}P < 0.01$, $^{***}P < 0.001$.

can prevent the severe secondary damage to neurons caused by the leakage of toxic substances and inflammatory factors from the blood into the brain parenchyma. A series of *in vivo* experiments were conducted to investigate the effect of MSCo/miR-132-3p on secondary brain injury (Supporting Information Fig. S14A and S14B). We used 2,3,5-triphenyl tetrazolium chloride (TTC) staining to evaluate the brain lesion in tMCAO mice after 48 h of various formulations administration. The MSCo/miR-132-3p-treated tMCAO mice exhibited the least brain lesion, which was ascribed to the timely protective effect on BMECs and the reduction of BBB permeability (Fig. 6A and B, Supporting Information Fig. S15A). At the same time, the mildest brain edema was also observed in the MSCo/miR-132-3p group (Fig. S15B). Furthermore, the cellular oxidative stress levels in ischemic brain regions were probed by DCFH-DA, and a significant elevation of ROS was observed in the injured hemisphere of tMCAO mice, while only modest ROS was detected after treatment with MSCo/miR-132-3p (Fig. 6C and D). Furthermore, we examined the levels of malondialdehyde (MDA), a degradation product of lipid peroxide, in brain tissues using an ELISA kit.

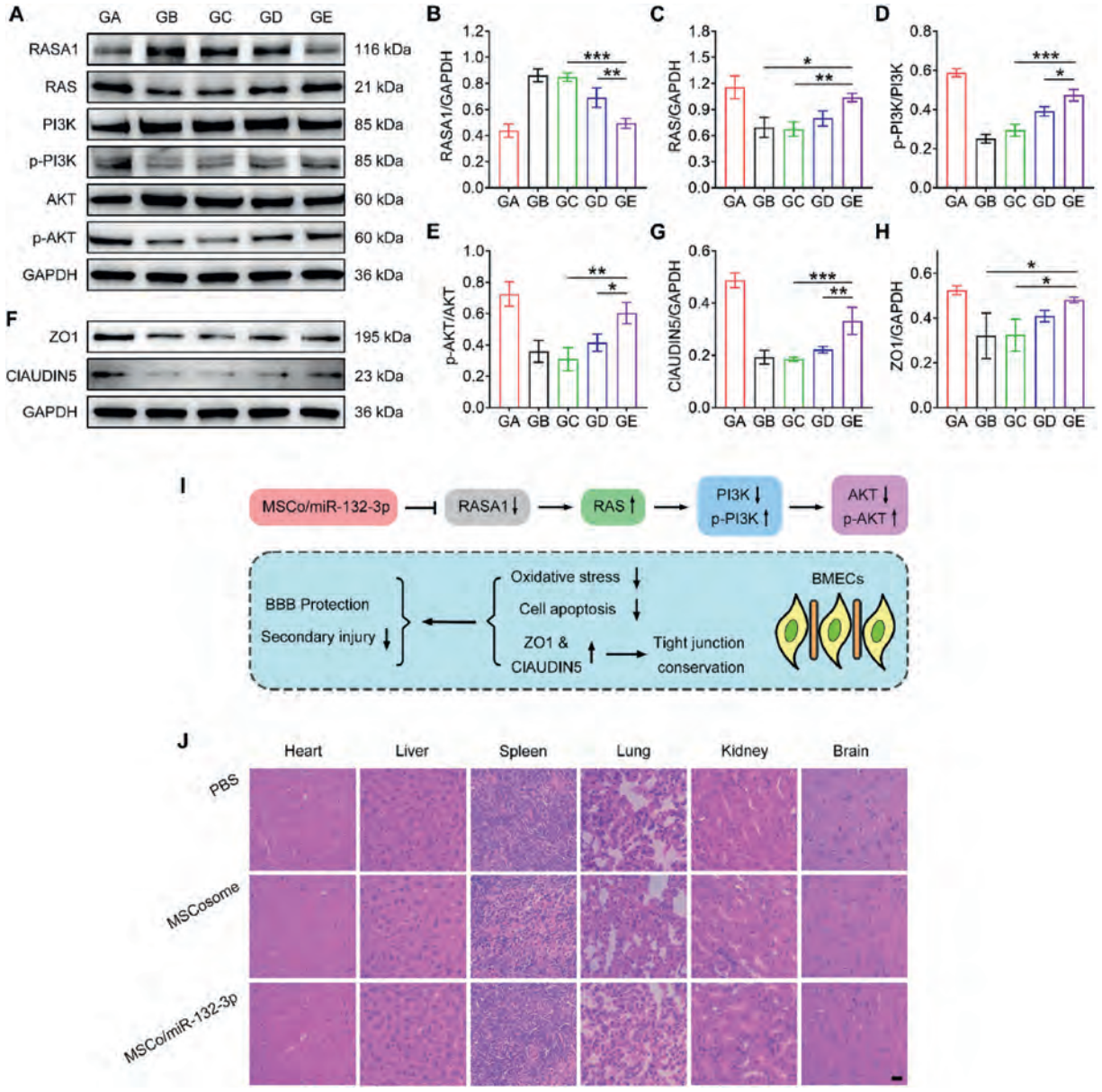

Figure 7 The action pathway and biocompatibility of MSCo/miR-132-3p. (A) Western-blot analysis of RASA1, RAS, PI3K, p-PI3K, AKT, p-AKT, and GAPDH (loading control) in the infracted hemisphere given different formulations. Group: GA: Sham; GB: PBS; GC: Naked miR-132-3p; GD: MSCosome; GE: Lipo/miR-132-3p; GF: MSCo/miR-132-3p. (B−E) The expression was analyzed as RASA1/GAPDH, RAS/GAPDH, p-PI3K/PI3K, and p-AKT/AKT ($n = 3$). (F−H) Western-blot analysis and quantification of tight junction proteins ZO1 and CLAUDIN5 in the infracted brain ($n = 3$). (I) Schematic representation of the pathway and downstream effects of MSCo/miR-132-3p. (J) H&E staining of major organs (heart, liver, spleen, lungs, kidneys, and brain) of healthy mice receiving different preparations. Scale bar, 20 μm. Data are presented as mean ± SD. Data are presented as mean ± SD. $^{*}P < 0.05$, $^{**}P < 0.01$, $^{***}P < 0.001$.

MSCo/miR-132-3p artificial vesicles can significantly reduce the level of MDA in the injured brain of MCAO mice (Supporting Information Fig. S16). The TUNEL staining results showed the same trend that the inhibitory effect of MSCo/miR-132-3p on apoptosis of the ischemic-injured brain cells was superior to that of the other groups (Fig. 6E and F). Altogether, these results demonstrated that the beneficial effects of MSCo/miR-132-3p on BMECs and BBB contributed to attenuating the secondary damage resulting from BBB disruption. Further, we examined the infiltration of immune cells in the ischemic brain. The results showed that the repaired BBB prevented the penetration of neutrophils and macrophages (Supporting Information Fig. S17A and S17B). Neuronal staining showed significantly improved neuronal survival in the MSCo/miR-132-3p group, which was attributed to reduced BBB permeability reducing immune cell infiltration during reperfusion, thus limiting the progression of neuroinflammation (Supporting Information Fig. S18). Next, another batch of tMCAO mice was injected with MSCo/miR-132-3p artificial vesicles every other day for 7 days to investigate whether it has a sustained effect against ischemia stroke. It was shown that the MSCo/miR-132-3p treatment group had the smallest area with structural loosening and destruction detected by

hematoxylin and eosin (H&E) staining (Fig. 6G). In addition, MSCo/miR-132-3p-treated mice were free from death within 7 days (Fig. 6H), maintained a normal weight growth trend (Supporting Information Fig. S19A), and exhibited better neurological function scores and locomotor ability compared with other groups (Fig. 6I and J, Fig. S19B). Finally, we compared the efficacy of artificial and natural MSC extracellular vesicles. We extracted natural MSC vesicles by gradient centrifugation, which have a diameter of about 150 nm and show a typical vesicle-like structure (Supporting Information Fig. S20A and S20B). tMCAO mice were given natural vesicles and artificial vesicles, respectively, and the efficacy was evaluated. According to neurological function scores and TTC staining results, natural vesicles had certain effects on the improvement of nerve function and the reduction of cerebral infarction area of tMCAO mice, but not as obvious as artificial vesicles (Fig. S20C and S20D). This may be due to the low content of therapeutic miR-132-3p in natural vesicles and the high loading of miR-132-3p in artificial vesicles, which achieve effective enrichment in BMECs. In general, the MSC membrane biomimetic artificial vesicles constructed in this study have a similar size and shape to that of natural MSC vesicles, but due to the controllable regulation of MSC membrane protein content and miRNA content, artificial vesicles have superior targeting and therapeutic effects to natural vesicles.

3.6. Mechanism and biocompatibility of MSCo/miR-132-3p

RASA1 is a GTPase-activating protein situated in the cytoplasm that suppresses the activity of RAS, the expression of which in BMECs can be down-regulated by miR-132-3p to inhibit mortality and facilitate angiogenesis[18]. As Western blot assay verified, the RASA1 concentration was significantly lower in the brain tissues of the MSCo/miR-132-3p-treated mice compared to the PBS-treated and naked miR-132-3p-treated group mice, resulting in significantly increased RAS expression, whereas Lipo/miR-132-3p was not as effective as MSCo/miR-132-3p, due to the absence of targeting properties (Fig. 7A−C). The upregulation of RAS—a recognized activator of the PI3K/AKT pathway—induced by MSCo/miR-132-3p promoted downstream phosphorylation of PI3K and AKT (Fig. 7A, D, and E). Through the RASA1/RAS/PI3K/AKT signaling pathway, MSCo/miR-132-3p attenuated excessive ROS generation and apoptosis in BMECs. Furthermore, it was confirmed that MSCo/miR-132-3p reduced the degradation of tight junction protein (Zona Occludens 1 (ZO1) and CLAUDIN5) in tMCAO mice brain through the aforementioned signaling pathway (Fig. 7F−H). In summary, the mechanism of the therapeutic effect of MSCo/miR-132-3p artificial vesicles on BMECs and BBB is described in Fig. 7I.

Finally, the preliminary *in vivo* biocompatibility of MSCo/miR-132-3p was studied. After tail vein administration of MSCosome and MSCo/miR-132-3p for 14 consecutive days, the body weights of mice were recorded to exhibit a steady growth trend (Supporting Information Fig. S21A). The major organs (heart, liver, spleen, lung, kidney, and brain) were harvested for weighing and HE staining, and no significant abnormality was observed compared with the control group (Fig. S21B, Fig. 7J). Besides, the hematological and biochemical analyses showed no remarkable discrepancy in the index parameters between the MSCosome or MSCo/miR-132-3p group and the PBS group (Fig. S21C−S21J, Supporting Information Table S6). In summary, it is indicated that the MSCosome and MSCo/miR-132-3p artificial extracellular vesicles have excellent biocompatibility.

4. Conclusions

In this study, we constructed a novel artificial MSC extracellular vesicles using both "top-down" and "bottom-up" strategies for targeted delivery of miR-132-3p to BMECs and demonstrated its role in counteracting oxidative stress and apoptosis of BMECs, as well as diminishing BBB permeability and secondary brain damage. miR-132-3p avoided rapid degradation due to the shielding of artificial MSC extracellular vesicles and achieved lysosomal escape *via* the DOPE H_{II} phase transition. The insertion of MSCs-associated membrane proteins endowed MSCo/miR-132-3p to evade immunosurveillance, prolong circulation time, and selectively migrate and adhere to BMECs. Remarkably, by taking advantage of both "top-down" and "bottom-up" synthesis strategies to fabricate MSCosome, it can be argued that various artificial extracellular vesicle delivery systems can be established in the future for different disease treatments.

Acknowledgments

This study was supported by the National Science Foundation of China (82473862 and 82304414), the open fund of National Key Laboratory of Advanced Drug Formulations for Overcoming Delivery Barriers (2024-KFA-007, China), Top Talent Support Program for young and middle-aged people of Wuxi Health Committee (HB2023103, China), Wuxi Young Science and Technology Talent Support Program (TJXD-2024-107, China), Key Science Foundation of Jiangyin Health Committee (K202101, China).

Author contributions

Shengnan Li: Conceptualization, Data curation, Formal analysis, Methodology, Writing - original draft, Visualization. Wei Lv: Formal analysis, Funding acquisition, Writing - review & editing. Jiangna Xu: Software, Investigation. Jiaqing Yin: Formal analysis, Investigation. Yuqin Chen: Investigation. Linfeng Liu: Investigation. Xiang Cao: Conceptualization. Wenjing Li: Investigation. Zhen Li: Resources, Supervision. Hua Chen: Project administration, Writing - review & editing. Hongliang Xin: Conceptualization, Funding acquisition, Resources, Project administration, Supervision, Data curation, Writing - review and editing.

Conflicts of interest

The authors declare no conflicts of interest.

Appendix A. Supporting information

Supporting information to this article can be found online at https://doi.org/10.1016/j.apsb.2025.06.009.

References

1. Tsao CW, Aday AW, Almarzooq ZI, Alonso A, Beaton AZ, Bittencourt MS, et al. Heart disease and stroke statistics-2022 update: a report from the American Heart Association. *Circulation* 2022;**145**: e153−639.
2. Emberson J, Lees KR, Lyden P, Blackwell L, Albers G, Bluhmki E, et al. Effect of treatment delay, age, and stroke severity on the effects of intravenous thrombolysis with alteplase for acute ischaemic stroke:

a meta-analysis of individual patient data from randomised trials. *Lancet* 2014;**384**:1929−35.
3. Liberale L, Gaul DS, Akhmedov A, Bonetti NR, Nageswaran V, Costantino S, et al. Endothelial SIRT6 blunts stroke size and neurological deficit by preserving blood−brain barrier integrity: a translational study. *Eur Heart J* 2020;**41**:1575−87.
4. Li Y, Liu B, Zhao T, Quan X, Han Y, Cheng Y, et al. Comparative study of extracellular vesicles derived from mesenchymal stem cells and brain endothelial cells attenuating blood−brain barrier permeability *via* regulating Caveolin-1-dependent ZO-1 and Claudin-5 endocytosis in acute ischemic stroke. *J Nanobiotechnol* 2023;**21**:70.
5. Fu Y, Liu Q, Anrather J, Shi FD. Immune interventions in stroke. *Nat Rev Neurol* 2015;**11**:524−35.
6. Wu JR, Hernandez Y, Miyasaki KF, Kwon EJ. Engineered nanomaterials that exploit blood−brain barrier dysfunction for delivery to the brain. *Adv Drug Deliv Rev* 2023;**197**:114820.
7. Li Q, Niu X, Yi Y, Chen Y, Yuan J, Zhang J, et al. Inducible pluripotent stem cell-derived small extracellular vesicles rejuvenate senescent blood−brain barrier to protect against ischemic stroke in aged mice. *ACS Nano* 2023;**17**:775−89.
8. Sun J, Huang Y, Gong J, Wang J, Fan Y, Cai J, et al. Transplantation of hPSC-derived pericyte-like cells promotes functional recovery in ischemic stroke mice. *Nat Commun* 2020;**11**:5196.
9. Eltzschig HK, Carmeliet P. Hypoxia and inflammation. *N Engl J Med* 2011;**364**:656−65.
10. Iadecola C, Anrather J. The immunology of stroke: from mechanisms to translation. *Nat Med* 2011;**17**:796−808.
11. Gong S, Cao G, Li F, Chen Z, Pan X, Ma H, et al. Endothelial conditional knockdown of NMMHC IIA (Nonmuscle Myosin Heavy Chain IIA) attenuates blood−brain barrier damage during ischemia−reperfusion injury. *Stroke* 2021;**52**:1053−64.
12. Rawal S, Munasinghe PE, Shindikar A, Paulin J, Cameron V, Manning P, et al. Down-regulation of proangiogenic microRNA-126 and microRNA-132 are early modulators of diabetic cardiac microangiopathy. *Cardiovasc Res* 2017;**113**:90−101.
13. Zhang ZS, Liu YY, He SS, Bao DQ, Wang HC, Zhang J, et al. Pericytes protect rats and mice from sepsis-induced injuries by maintaining vascular reactivity and barrier function: implication of miRNAs and microvesicles. *Mil Med Res* 2023;**10**:13.
14. Xu B, Zhang Y, Du XF, Li J, Zi HX, Bu JW, et al. Neurons secrete miR-132-containing exosomes to regulate brain vascular integrity. *Cell Res* 2017;**27**:882−97.
15. McCormick F. Ras GTPase activating protein: signal transmitter and signal terminator. *Cell* 1989;**56**:5−8.
16. Henkemeyer M, Rossi DJ, Holmyard DP, Puri MC, Mbamalu G, Harpal K, et al. Vascular system defects and neuronal apoptosis in mice lacking ras GTPase-activating protein. *Nature* 1995;**377**:695−701.
17. Hershkovitz D, Bercovich D, Sprecher E, Lapidot M. RASA1 mutations may cause hereditary capillary malformations without arteriovenous malformations. *Br J Dermatol* 2008;**158**:1035−40.
18. Anand S, Majeti BK, Acevedo LM, Murphy EA, Mukthavaram R, Scheppke L, et al. MicroRNA-132-mediated loss of p120RasGAP activates the endothelium to facilitate pathological angiogenesis. *Nat Med* 2010;**16**:909−14.
19. Katare R, Riu F, Mitchell K, Gubernator M, Campagnolo P, Cui Y, et al. Transplantation of human pericyte progenitor cells improves the repair of infarcted heart through activation of an angiogenic program involving micro-RNA-132. *Circ Res* 2011;**109**:894−906.
20. Pan Q, Kuang X, Cai S, Wang X, Du D, Wang J, et al. miR-132-3p priming enhances the effects of mesenchymal stromal cell-derived exosomes on ameliorating brain ischemic injury. *Stem Cell Res Ther* 2020;**11**:260.
21. Chaudhary V, Jangra S, Yadav NR. Nanotechnology based approaches for detection and delivery of microRNA in healthcare and crop protection. *J Nanobiotechnol* 2018;**16**:40.
22. Yu AM, Choi YH, Tu MJ. RNA drugs and RNA targets for small molecules: principles, progress, and challenges. *Pharmacol Rev* 2020;**72**:862−98.
23. Carreras-Badosa G, Maslovskaja J, Periyasamy K, Urgard E, Padari K, Vaher H, et al. NickFect type of cell-penetrating peptides present enhanced efficiency for microRNA-146a delivery into dendritic cells and during skin inflammation. *Biomaterials* 2020;**262**:120316.
24. Michell DL, Vickers KC. HDL and microRNA therapeutics in cardiovascular disease. *Pharmacol Ther* 2016;**168**:43−52.
25. Li J, Wang T, Hou X, Li Y, Zhang J, Bai W, et al. Extracellular vesicles: opening up a new perspective for the diagnosis and treatment of mitochondrial dysfunction. *J Nanobiotechnol* 2024;**22**:487.
26. Zeng B, Li Y, Khan N, Su A, Yang Y, Mi P, et al. Yin−Yang: two sides of extracellular vesicles in inflammatory diseases. *J Nanobiotechnol* 2024;**22**:514.
27. Shao H, Im H, Castro CM, Breakefield X, Weissleder R, Lee H. New technologies for analysis of extracellular vesicles. *Chem Rev* 2018;**118**:1917−50.
28. Kumar MA, Baba SK, Sadida HQ, Marzooqi SA, Jerobin J, Altemani FH, et al. Extracellular vesicles as tools and targets in therapy for diseases. *Signal Transduct Targeted Ther* 2024;**9**:27.
29. van Niel G, D'Angelo G, Raposo G. Shedding light on the cell biology of extracellular vesicles. *Nat Rev Mol Cell Biol* 2018;**19**:213−28.
30. Wu HH, Zhou Y, Tabata Y, Gao JQ. Mesenchymal stem cell-based drug delivery strategy: from cells to biomimetic. *J Control Release* 2019;**294**:102−13.
31. Ma J, Zhang S, Liu J, Liu F, Du F, Li M, et al. Targeted drug delivery to stroke *via* chemotactic recruitment of nanoparticles coated with membrane of engineered neural stem cells. *Small* 2019;**15**:e1902011.
32. Zhang M, Hu S, Liu L, Dang P, Liu Y, Sun Z, et al. Engineered exosomes from different sources for cancer-targeted therapy. *Signal Transduct Targeted Ther* 2023;**8**:124.
33. Wang S, Birch PRJ, Jin H. Extracellular vesicles: a new avenue for mRNA delivery. *Trends Plant Sci* 2024;**29**:845−7.
34. Usman WM, Pham TC, Kwok YY, Vu LT, Ma V, Peng B, et al. Efficient RNA drug delivery using red blood cell extracellular vesicles. *Nat Commun* 2018;**9**:2359.
35. Herrmann IK, Wood MJA, Fuhrmann G. Extracellular vesicles as a next-generation drug delivery platform. *Nat Nanotechnol* 2021;**16**:748−59.
36. Molinaro R, Corbo C, Martinez JO, Taraballi F, Evangelopoulos M, Minardi S, et al. Biomimetic proteolipid vesicles for targeting inflamed tissues. *Nat Mater* 2016;**15**:1037−46.
37. Chaudhary N, Weissman D, Whitehead KA. mRNA vaccines for infectious diseases: principles, delivery and clinical translation. *Nat Rev Drug Discov* 2021;**20**:817−38.
38. Zhang Y, Sun C, Wang C, Jankovic KE, Dong Y. Lipids and lipid derivatives for RNA delivery. *Chem Rev* 2021;**121**:12181−277.
39. Eygeris Y, Gupta M, Kim J, Sahay G. Chemistry of lipid nanoparticles for RNA delivery. *Acc Chem Res* 2022;**55**:2−12.
40. Ruster B, Gottig S, Ludwig RJ, Bistrian R, Muller S, Seifried E, et al. Mesenchymal stem cells display coordinated rolling and adhesion behavior on endothelial cells. *Blood* 2006;**108**:3938−44.
41. Chamberlain G, Fox J, Ashton B, Middleton J. Concise review: mesenchymal stem cells: their phenotype, differentiation capacity, immunological features, and potential for homing. *Stem Cell* 2007;**25**:2739−49.
42. Olsson M, Oldenborg PA. CD47 on experimentally senescent murine RBCs inhibits phagocytosis following Fcgamma receptor-mediated but not scavenger receptor-mediated recognition by macrophages. *Blood* 2008;**112**:4259−67.
43. Oldenborg PA, Zheleznyak A, Fang YF, Lagenaur CF, Gresham HD, Lindberg FP. Role of CD47 as a marker of self on red blood cells. *Science* 2000;**288**:2051−4.